Master Thesis

Design and Optimization of a Patient-Specific Additively Manufactured Subperiosteal Ceramic Implant

carried out for the purpose of obtaining the degree of Master of Science (Dipl.-Ing.), submitted at TU Wien, Faculty of Mechanical and Industrial Engineering, by

Daniel Alexander Aigner

Mat.Nr.: 01228808

under the supervision of:

Univ.Prof. Dipl.-Ing. Dr.techn. Dieter Pahr

Institute of Lightweight Design and Structural Biomechanics at TU Wien

and

Assoc. Prof. Dipl.-Ing. Francesco Moscato, PhD

Center for Medical Physics and Biomedical Engineering at Medical University of Vienna

Vienna, September 2022

Affidavit

I declare in lieu of oath, that I wrote this thesis and performed the associated research myself, using only literature cited in this volume. If text passages from sources are used literally, they are marked as such.

I confirm that this work is original and has not been submitted elsewhere for any examination, nor is it currently under consideration for a thesis elsewhere.

I acknowledge that the submitted work will be checked electronically-technically using suitable and state-of-the-art means (plagiarism detection software). On the one hand, this ensures that the submitted work was prepared according to the high-quality standards within the applicable rules to ensure good scientific practice "Code of Conduct" at the TU Wien. On the other hand, a comparison with other student theses avoids violations of my personal copyright.

_____   _____

City and Date   Signature

Acknowledgements

First I would like to acknowledge and express my deepest gratitude to Assoc. Prof. Dipl.-Ing. Francesco Moscato, PhD for his invaluable patience and feedback. Further, I would like to extend my sincere thanks to Univ.Prof. Dipl.-Ing. Dr.techn. Dieter Pahr, who generously provided knowledge and expertise.

I am extremely grateful to have worked together with Dr. Gunpreet Oberoi, PhD, without whom this thesis would not have been possible. Moreover, I'd like to recognize Dipl.-Ing. Erik Kornfellner, BSc, for his valuable input.

I am also grateful to my friends in room 18, Lorenzo, Marta and Laurenz, with whom I laughed and who created such a wonderful working environment.

Finally, I would like to take this opportunity to express my sincere gratitude to my family, especially my parents Monika and Peter, my brother Christof, my aunt Elisabeth, my grandmother Margaretha, posthumously my grandfather Hermann, and Stephan. Without them, I would not have been able to accomplish any of this. Your trust in me and the deep bond between us have led to a truly wonderful journey that does not end here.

Abstract

Objective: To design and optimize a patient-specific subperiosteal maxillary implant in 3D-printed Yttrium-stabilized Zircon oxide by utilizing topological optimisation (TO) for assigning lattices to improve osseointegration and load bearing, while reducing the bulk of the implant.

Materials & Methods: A contrast-based segmented skull model from an anonymized computed tomography data of a patient was used for this research. A maxillary subperiosteal implant was initially designed according to the available residual bone. This initial implant was then processed for TO under different load bearing conditions. Structural modifications and lattice incorporation were performed according to the TO and the final design underwent in-silico biomechanical evaluation.

Results: This study resulted in two different types of patient-specific subperiosteal maxillary implants, a) initial design based on the available bone, b) redesign on the basis of TO and an osseoconductive lattice. The in-silico tensile test revealed that the Young's modulus of the lattice structure incorporated into the implant is 83,3 GPa in contrast to that of the yttrium-stabilized ceramic bulk material which is 205 GPa. The absolute maximum principal stresses in the implant were considered, leading to 61,14 MPa in the bulk material and 278,63 MPa in the lattice, both tolerable by the bulk material and the lattice, suggesting that the redesigned implant can resist the occlusal forces (125-250 N per abutment).

Conclusion: This thesis showed the potential to use TO to advance the patient-specificity of a dimensionally customised 3D-printed implant. However, experimental validation of the proposed workflow is necessary towards a clinical implementation of the proposed implant design.

Kurzfassung

Ziel: Das Design und die Optimierung eines patientenspezifischen subperiostalen Implantats für die Maxilla aus einer 3D-gedruckten Yttrium-stabilisierten Keramik an derer die Methode der Topologieoptimierung (TO) für die Zuweisung einer Gitterstruktur angewandt wird um das Implantat bezüglich Osseointegration und Belastbarkeit bei gleichzeitiger Verringerung der Masse zu verbessern.

Methodik: Für diese Studie wurde ein bereits segmentiertes Schädelmodel aus anonymisierten computertomographischen-Daten eines Patienten verwendet. Ein initiales subperiostales Oberkieferimplantat wurde entsprechend des verfügbaren Restknochens entworfen. Dieses initiale Implantat wurde dann für TO unter verschiedenen Belastungsbedingungen aufbereitet. Strukturelle Änderungen und der Einbau von Gitterstrukturen wurden entsprechend der TO durchgeführt, und das endgültige Design wurde einer biomechanischen in-silico-Evaluierung unterzogen.

Ergebnisse: Die durchgeführte Studie hat zwei verschiedene Arten von patientenspezifischen subperiostalen Oberkieferimplantaten ergeben: a) ein ursprüngliches Design auf der Grundlage des vorhandenen Knochens und b) ein Redesign auf der Grundlage von TO und einem osseokonduktiven Gitter. Der In-silico-Zugversuch ergab, dass der Elastizitätsmodul des in das Implantat eingebauten Gitters 83,3 GPa beträgt, im Gegensatz zu dem des Yttrium-stabilisierten keramischen Vollmaterials, das 205 GPa beträgt. Die absoluten maximalen Hauptnormalspannungen im Implantat wurden untersucht und ergaben 61,14 MPa im Vollmaterial und 278,63 MPa in der Gitterstruktur, die sowohl vom Vollmaterial als auch von der Gitterstruktur ertragen werden können, was darauf hindeutet, dass das neu gestaltete Implantat den okklusalen Kräften (125-250 N pro Abutment) standhalten kann.

Schlussfolgerungen: In dieser Arbeit wurde das Potenzial der TO zur Verbesserung der Patientenspezifität eines individuell gestalteten 3D-gedruckten Implantats aufgezeigt. Eine experimentelle Validierung des beschriebenen Arbeitsablaufs könnte das vorgeschlagene Implantatdesign jedoch noch verbessern.

Contents

Abbrevations

AM	Additive Manufacturing
BC	Boundary Condition
CAD	Computer Aided Design
CBCT	Cone Beam Computed Tomography
CT	Computed Tomography
DLP	Digital Light Processing
DMLS	Direct Metal Laser Sintering
DOF	Degree of Freedom
FE	Finite Element
FEM	Finite Element Method
FH	Frankfort Horizontal
IBO	Inferior Border of the Orbitale
LCM	Lithography-based Ceramic Manufacturing
LP	Lip Plane
MRI	Magnetic Resonance Imaging
OP	Occlusion Plane
PP	Porion Point
RBE	Rigid Body Element
RP	Rapid Prototyping
SLA	Stereolithography
SLM	Selective Laser Melting
SPC	Single Point Constraint
THA	Total Hip Arthorpolasty
TKA	Total Knee Arthroplasty
TO	Topology Optimization

Symbols

A	Area
$BaTiO_3$	Barium Titanate
CaO	Calcium Oxide
c_{equ}	Equivalent Spring Stiffness
E	Young's Modulus
E_{eff}	Effective Young's Modulus

(continued)

Contents

E_i	Reduced Young's modulus
$E_{i,0}$	Young's modulus of the starting material
E_0	Young's modulus of the bulk material
$\underline{F}$	Nodal Force
F_z	z-component of Resulting Force
$\underline{\underline{K}}$	Element Stiffness Matrix
k	Parameter Describing the Morphology of the Pores
l	Cube length
$MgAl_2O_4$	Spinel
MgO	Magnesium Oxide
p	Penalization Exponent
p_c	Porosity at which the Young's Modulus becomes zero
r	Stress Magnification Factor
r_{new}	Adjusted Stress Magnification Factor
ρ_i	Computed Tomography
$\rho_{i,0}$	Material Density of Solid Element
σ	Material Density assigned to the Element
σ_{mid}	Average Stress
σ_{max}	Maximum Stress
$\tilde{\sigma}_{max}$	Adjusted Maximum Stress
u	Displacement
$\underline{U}$	Displacement Vector
x_i	Design Variable
Y_2O_3	Yttrium Oxide
$ZnFe2O_4$	Zinc Ferrite
ZrO_2	Zirconium Oxide

1 Introduction

1.1 Motivation

Dental implants are a well-established treatment of choice for restoring edentulism.[1] As being prevalent in approximately 352 million cases worldwide, edentulism presents a significant medical and economical burden.[2, 3] Depending on the pre-existing medical conditions, the residual ridge and the patients' desire, the type of dental implant can be selected.[4] Advances in the manufacturing process of implants, however, with the technology of additive manufacturing (AM) and improved imaging methods as computed tomography (CT), and cone-beam computed tomography (CBCT) give the possibility of designing patient-specific implants.[5] In addition, treatment concepts such as the subperiosteal implant are experiencing a renaissance, as patient-specific use leads to an improved and desirable outcome that could not be achieved with earlier, conventionally manufactured subperiosteal implants.[6, 7] This thesis proposes a workflow for designing a patient specific subperiosteal implant for the maxilla. To improve the design of the individualized implant, it is essential to acquire knowledge of the mechanical stresses in the bone and the implant. Bone is a living tissue that remodels as a response to external loads, defined by Wolff's law.[8] Consequently, implants can lead to an alteration in the internal stresses experienced by the bone. If the implant absorbs an abnormal high amount of stress, then this could result in a loss of bone mass in the environment which is only affected by a diminished portion of the stress. This effect is called stress shielding and may cause mechanical loosening of the implant.[9] To mitigate this unwanted effect, the implant should be designed in a way that the bone is exposed to a physiological stress distribution. Therefore, obtaining these stress results directly influence the design of the implant. To study these stress distributions, the finite element method (FEM), often used in biomedical applications, can be employed.[10, 11] The FEM reduces the complexity of the mechanical problem by dividing it into smaller and simpler elements. So, instead of acquiring the solution for the mechanical problem for the whole system at once, the problem is computationally solved for each element.[10]

Another potential improvement to an initial implant design based on FEM considerations holds the field of topology optimization (TO).[12] TO draws great attention due to the high

potential achievable economical savings for the industry.[13, 14] In addition, TO developed to a powerful approach under medical implant designers to attain a biomechanically improved product regarding the principle of finding the ideal material distribution at the basis of the FEM.[15] TO has also been used for improving a patient specific subperiosteal implant regarding the macro-structure.[16] Since the TO method has already been well established in implant design, the questions arises, if there are other facets to or potential use-cases for this method.

Osseointegration is also important in the context of implant design. This term refers to the process of the formation of a structural and functional compound between a living bone tissue and the surface of an adjacent implant.[17] It is the result of the bone's healing process, where bone cells attach to the implant surface and result in a solid anchorage.[17] This process can be promoted by the implant's macro- and micro-structure[18]. A lattice, for example, which is represented by an arrangement of beams, can promote osseointegration.[19] Therefore, in this research TO has been applied to identify the regions within the implant where the bulk material can be substituted by a lattice. This makes the AM-based FEM and TO-guided implant design precise and tailored to the individual-oral stresses.

While this approach to precision medicine is widely implemented in contemporary implant dentistry, case reports show only a limited number of materials currently available.[20, 21] Owing to their excellent corrosion resistance, metal alloys like Ti-6Al-4V have been broadly used, but, complications in bone mineralization or allergic reactions could occur due to the possibility of the alloy releasing aluminium and vanadium.[22] Therefore, it is of great interest to investigate different potential materials for implants. Moreover, biomechanical improvements for titanium implants are demonstrated in the literature.[22] As high performance ceramic implants are well established in total hip arthroplasty (THA) and total knee arthroplasty (TKA), a potential use case in subperiosteal implant design could arise.[23] Zirconia ceramics are characterized by a lower risk of fractures as conventional ceramics, which again could be beneficial.[23] Given this knowledge, a yttrium-stabilized zirconium ceramic material appears as potential candidate for investigating the stresses occurring in the implant.

1.2 Edentulism

Edentulism is still an ongoing challenge in the whole world.[24] It is a severe form of tooth loss and defined by the total loss of teeth within the oral cavity, usually accompanied by a deterioration of the quality of life of the affected person.[3] According to the Global burden of Disease Study 2019, 3,5 billion people are confronted with an oral condition, with severe tooth loss and edentulism being prevalent in approximately 352 million cases.[2] This high

number of cases go along with a great economic burden as the treatment of oral diseases make up for about 4,7% of the yearly global health expenditure.[3] Due to profound disparities in the health care system between developed and developing countries, the latter is facing a harder challenge to counteract oral diseases.[25] Given a greater health care system, a downwards trend of edentulous persons in Europe can be identified over the last 30 years, while numbers in developing countries are still increasing.[26] With 30% of older Europeans, who are in the age group of 65-74, affected with severe or total loss of their natural teeth, the potential for improvement is apparent.[27] In the United States of America, about 26% of adults being in the age group over 65 years have 8 or fewer teeth and about 17% have lost all of their teeth.[28, 29] Additionally, it can be stated, that older adults in the US, who are living in poverty, have a minor school education, or are cigarette smokers raise the chance the chance to loose all their teeth 3 times.[29] A downwards trend towards fewer cases as in Europe regarding edentulism, however, can be identified.[29]

1.2.1 Causalities and Consequences

The causalities with edentulism are manifold. Studies show a correlation between tooth loss and obesity and vice versa.[3] It can be stated, that fat tissue promotes various diseases due to the high concentrations of bioactive substances like prototypic adipocytokines, which are functioning like hormones in the surroundings of fat tissue. Some of these seem to have a pro-inflammatory effect.[30] Therefore, obese individuals have a higher probability to be affected by periodontal disease. Periodontitis is an irreversible inflammation of the oral mucosa, which can be seen as a fundamental cause for tooth loss.[3, 31]. Periodontitis, however, is preventable by lifelong daily plaque removal and lifestyle changes as e.g. quitting smoking.[32] Daily tooth brushing is still seen as the most important precaution against periodontitis, since the gathering of plaque at the oral mucosa introduces an inappropriate and destructive inflammation of the body.[32] Additionally, it is demonstrated, that periodically undergone professional oral prophylaxis benefit the oral health which is associated with the reduction of plaque.[32]

Nevertheless, persons with missing teeth showed a higher likelihood of being obese and edentulous persons showing even a higher likelihood for it. Since missing teeth influence an individuals' mastication, studies showed that affected people would alter there nourishment variety. Consequently, studies demonstrated the effect of missing teeth on the quality and type of diet. It was reported that edentulism is linked to a lower intake of vegetables, fruits and dietary fibres.[3] Thus, the integrity of the oral cavity is a major factor regarding malnutrition.[33]

A systematic review and meta-analyses provided by Cademartori et al. in 2018 showed a

correlation between depression and edentulism in adults and elders.[34] Hence, edentulism seems to enlarge the chance of following depressive symptoms.[34] Additionally, dental and oral health in general have an influence on the person's self-esteem, due to the impact on an individual's attractiveness.[35] Moreover, physical and facial attractiveness take part in human interactions, therefore, impacts friendships or the outcome of finding a significant other. The correlation between self-assessment of attractiveness and mental stability or anxiety is reported.[35]

Another aspect is the influence of education on oral health. A hypothesis about education being a positive influence on the individuals' oral health is the enhanced ability to understand cause and effect relations. Therefore, higher educated people are more likely to maintain a healthier life, since they would rather choose the healthier option. It was demonstrated, that every additional year of education result in the decrease of 9% points in the probability of edentulism.[36]

Since periodontitis can lead to teeth loss, it is apparent to enlighten the risk factors for periodontitis.[37] One major disease that is linked to this periodontal disease is diabetes mellitus.[38] Diabetes mellitus is a metabolic disease spectrum associated to the malfunction of the bodies sugar regulation.[39] Periodontitis and diabetes mellitus have many risk factors in common, as smoking, alcohol abuse, obesity, lack of physical exercise and high refined sugar intake. Therefore, both diseases are highly likely to appear in the same individual. Periodontal diseases is on the other hand a risk factor for deteriorating diabetes mellitus itself and vice versa, so, they both influence the outcome of the treatment.[39] Another aspect of the potential risk of not treated edentulism gives the bone remodeling law by Wolff. Wolff's law states, that bone will remodel its architecture in relation to the forces applied.[8] Therefore, bone gets stronger, if it is exposed to constant high loads, or even deteriorate if loaded less or not at all. Consequently, if areas of the jaw or even the complete jaw is not exposed to loads anymore due to the lack of teeth, these areas are exposed to bone loss, leading to an alteration of the facial aesthetics.[40]

In addition, studies have linked edentulism with different serious health conditions, including an enhanced risk of developing chronic kidney disease, diabetes and heart conditions like hypertension[37, 38, 41, 42]. Hence, it is evident, that tooth loss needs quick and effective treatment in order to avoid permanent issues.

1.2.2 Curative Treatment for Edentulism

As stated before, edentulism and partial edentulism as well affects the body in different ways. Despite a single missing tooth will not lead to distinct practical obstacles at the beginning,

it is entirely reasonable, however, for the adjacent teeth to start moving towards the opened space, resulting in the possibility of introducing occlusal problems.[43]

The majority of patients are affected by a partial edentulous condition, meaning, they either are missing only a single tooth or a small number of teeth.[2] Replacing a missing tooth with dental implants, partial dentures, dental bridges or a combination of these, relative to the underlying edentulous pattern present, turned out to be one of the most effective measures for a patient in order to restore aesthetics and function.[44] It was already stated, that untreated edentulism is associated with bone loss. An acceptable volume of quality bone, however, is a prerequisite for a long lasting implant.[45] Additionally, the positioning of the implant is of great importance, since a misplaced implant can lead to peri-imlpantitis, which is an inflammation of the implant adjacent mucosa leading to loss of the supporting bone.[22, 46]. Peri-implantitis is the most prevalent cause for a titanium implant to fail.[22] Therefore, it is essential to choose the correct implant for the proper condition. There is a vast variety of implants available, and there is a possible classification regarding the implantation site in the oral cavity[18]:

Endosseous Implants

Endosseous or endosteal dental implants are intended to be implanted into the alveolar or basal bone of the maxilla or mandibula, while the implant's body stays embedded within the bone.[18] A prerequisite for the use of endosseous implants is sufficient bone quantity and quality.[21] This type of implant is designed to be an individual unit, therefore, the clinician has the possibility to select between different sizes and numbers of units which are placed in the patient's jaw in order to guarantee the best treatment result.[18] State of the art endosseous implants are provided with a macro-structure to enhance primary stability and a micro-structure to improve osseointegration.[18] Present statistics, however, show, that about 56% of the endosseous implants examined in the study displayed peri-implantitis, therefore, needed to be ex-planted.[7]

Eposteal and Subperiosteal Implants

The eposteal implant is a type of implant which is placed on top of the remaining jawbone, while securing the positioning with screws.[18] It is frequently used in cases of severe bone atrophy, where the use of endosseous implants is not applicable, like for patients of Cawood and Howell class V-VI bone atrophy.[7, 47] The subperiosteal implant is a form of eposteal

implant first introduced in 1942 by the Swedish dentist Dahl, primarily utilized for treating an edentulous mandible, since the mandible consists of a greater bone density as the maxilla, hence providing better support for the loads applied[18, 48].

In the implantation procedure, the operator retracts the oral mucosa and periosteum in order to expose the basal bone and places the implant subperiosteally, meaning under the periosteum, with a different number of abutments reaching through the oral mucosa for attaching the actual implant. Finally the periosteum and the oral mucosa are sutured to cover the bone and the implant.[18] Though the mandible consists of greater bone density as the maxilla, subperiosteal jaw implants can be used for treating both the mandible and the maxilla.[18] Associated maxillary bone deterioration, however, is a proven obstacle.[6] In addition, maintaining a proper bone-implant contact due to gravity is a challenge.[6] In earlier stages, the treatment of a patient with a subperiosteal implant was very complex, given the necessity of capturing the true surface of the residual bone with a prior surgery, inducing significant patient inconvenience.[21] Moreover, the accuracy and precision were far from exact, leading to a potential unexpected outcome.[21]

There have been major advancements in the area of subperiosteal implants: First, the concept of accompanied bone grafting in the mandible to enhance bone formation and osseointegration was introduced.[6] Bone grafting is a surgical procedure, where bone is cleaved to encourage bone formation in the context of guided bone regeneration.[45] One consequence of this technique, however, is the duration of treatment with the potential of complications during or after surgery, given the procedure's vast complexity.[21]

Second, the main material for subperiosteal implants used was originally the alloy vitallium, consisting of 65% cobalt, 30% chromium, 5% molybdenum, and other substances.[6] Today, grade 3 titanium is used for conventional subperiosteal implants.[6] Other materials like a hydroxyapatite and collagen nanocomposite-coating for titanium implants, however, appear to be related to advance osseointegration.[6, 49]

Third, the customization aspect due to the innovative possibilities given the technology of additive manufacturing is conveying new solutions, since shape optimizations can lead to refined bone-implant contact and improved biomechanical properties particularly for defects of the maxilla.[6] Furthermore, due to major improvements in the digital technology in medicine, new data gathering methods like CT lead to faster and better results. These advancements allow the renaissance of this implant concept.[50]

Transosteal Implants

These types of implants permeate the bone completely and are principally designed for the extremely atrophied mandibula.[18] Studies report positive results when treating with transosteal implants, comparison studies between transosteal and endosseous implants, however,

report significantly a superior outcome for endosseous implants for longer treatments than 1 year.[18]

Zygomatic and Pterygoid Implants

These implant types are placed either in the zygomatic or in the pterygoid processes.[18] Usually, both are less in use in routine procedures, zygomatic implants, however, have substituted the use of conventionally manufactured subperiosteal implants for the severly resorbed maxilla.[6, 21] The approach for the implantation of a zygomatic implant is to drill a transosseous path, which is highly risky due to a limited field of vision and possible damages to adjacent anatomical structures, with minor diversions leading to significant errors.[18] Clinical studies, however, report high success rates.[18] The pterygoid implant is another approach with drilling a transosseous path finally reaching the pterygoid process of the sphenoid bone.[18] The advantage of pterygoid implants is that the transosseous path is intended to be drilled in denser cortical bone to avoid a possible prior bone grafting procedure for shorter treatments.[18]

1.3 Anatomy of the Edentulous Maxilla

Since this thesis deals with the design of a subperiosteal maxilla implant, the focus in following text will be laid on this anatomical structure. The maxilla is formed of 2 maxillary bones, the maxillae, which are fused at the sutura intermaxillaris.[51] Both maxillae form the bony basis for the upper face and determine by their shape, size and position mainly the form of the midface. They participate in the formation of the walls of the orbital and nasal cavities and in the formation of the palate. They carry the upper row of teeth and, with a frontal and a zygomatic arch pillar, transfer the masticatory pressure to the cranium.[52]

Edentulous patients, however, suffer from bone atrophy, therefore less bone is available to transfer the occurring masticatory pressures to the cranium. Hence, for a subperiosteal implant which only rests on the bone, it is necessary to use the maximum available surface area. For the edentulous maxilla this is finite space of approximately 24 cm^2, since not the whole surface present may be used for implant.[54] The maxillary surface can be divided into stress-bearing and relief areas.[54] These anatomical landmarks are visualized in figure 1.1. There are stress-bearing areas that are supporting structures and may be loaded. These can be subdivided into primary and secondary stress-bearing areas, with the difference in the bone structure. The primary stress-bearing area generally consisting of cortical bone which
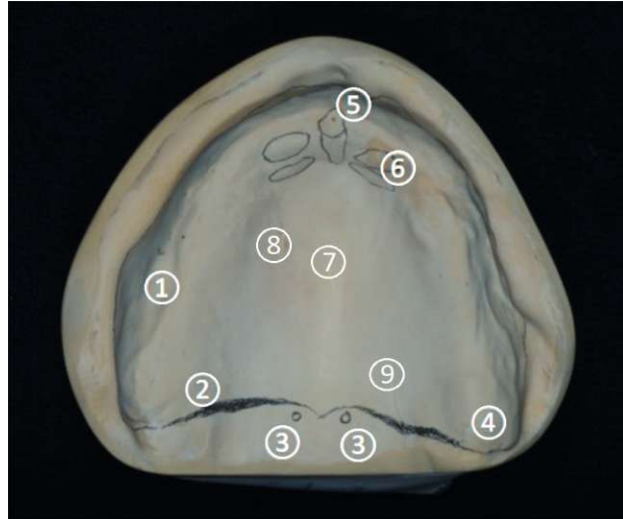
Figure 1.1: Anatomical Landmarks of an edentulous maxilla model. 1: residual alveolar ridge; 2: hamular notch; 3: fovea palatini; 4: maxillary tuberosity; 5: incisive papilla; 6: rugae; 7: palatine raphe; 8: hard palate; 9: posterior palate[53]

is less affected by resorption, whereas the secondary areas consist of trabecular bone, that is more affected by resorptive remodeling.[54] In the Maxilla, the primary stress-bearing areas are the firm tuberosities and the hard palate on either side of the palatal raphe as well as the posterior palate, numbers 4, 8 and 9 respectively in figure 1.1. The secondary stress-bearing areas are the alveolar ridge and the rugae, numbers 1 and 6.[54] Relief areas are regions which could resorb under pressure or cover fragile structures like nerves, therefore load should be avoided.[54] These are the incisive papilla which covers the fossa incisiva, the palatine raphe, which is the fusion line of the maxillae, and the fovea palatini, which mark the posterior limit, numbers 5, 7 and 3 in figure 1.1. The hamular notch, number 2, gives a limiting structure as well, so, the implant should not be extended any further to this point.[53]

1.4 Computer-Aided Implementation of Personalized Implants

All humans are different in terms of anthropometry and morphology.[5] Additionally, human tissues consist of various biological structures, like bone, skin, cartilage, etc. which again differ greatly in relation to their biomechanical properties.[55–57] Therefore, medicine is taking great effort in order to take all these differences into account to attain patient-specific treatment, called individualized/precision medicine.[5] The individualized treatment is suitable for one target patient, hence, others cannot benefit with the same patient-specific

product to achieve a comparable treatment. The concept of individualized medicine is not confined to a certain field in medicine, but is already implemented in various medical applications, for example, the curative treatment of edentulous people with patient specific dental implants.[7, 58–61]

A possible process chain for individualized medicine is initiated by the image acquisition.[5] To acquire the patient image data, magnetic resonance imaging (MRI) or CT is commonly used, with the aim to receive high quality images that allow an exact individual customization to the patient's anatomy. The cross-sectional image data set obtained from CT is divided into smaller segments. This usually involves converting voxels (spatial data set) into tetrahedrons, which is called segmentation. In this process, unnecessary information from the data set is discarded and only the data values of interest are retained. Various algorithms exist for segmentation, for example, data can be filtered according to their Hounsfield units, which are values for the attenuation of X-rays in different types of tissue. Ultimately, all of these algorithms should lead to a 3D anatomical model out of the 2D-images data stack of an anatomical segment of interest with a data volume less than that of the original data set.[62] The next step consists of building a computer-aided design (CAD) model of the segmented images. This CAD model can then be used for various scenarios. In the case of this thesis, the CAD model was used first to design an patient-specific implant and then to perform a biomechanical simulation. The CAD helps in producing a patient-specific design that should minimize the risk of potential complications, as severe osteolysis due to imperfect fit of the implant to the patient's anatomy.[5, 6] Furthermore, the stress distribution inside an implant and the bone can lead to different outcomes of a treatment.[12] To optimize the outcome, a biomechanical matched implant leading to physiologic-like stress distributions is necessary. To this end, numerical computation can be performed that require the reduction of complexity of the biomechanical problem. This can be done by dividing the computational domain into smaller entities, called finite elements (FEs). Solving the mechanical computation in these elements and combining the results together (e.g. stress distribution in the implant and/or bone) allows the designer to understand the biomechanical working condition and therefore provide a better fit of the implant for the patient's needs. In addition to analyzing the stress distribution, major improvements to an initial implant design can also be achieved by the TO method, which stems from the FEM.[15, 63] Especially in personalized medicine, due to the implied diversity and complexity in implant design, the benefit of computational modeling with FE is apparent.[5] The following chapter is dedicated to these two simulation methods.

1.4.1 Finite Element Method

The FEM was first used in implant dentistry by Tesk and Widera in 1973.[64] Ever since, it has become essential in the acquisition of stress distributions.[65] Nowadays, the FEM is the most used process for calculating stresses of complex structures.[66] Generally, the idea of the FEM is to approximate the analytical solution to a continuum mechanics problem of a complex body by dividing it into a finite number of elements, which is called discretization.[10] These problems are formulated by differential equations for each element, which address the underlying physics and consist of boundary conditions (BCs), that characterize the behaviour at the boundary. The FE are linked with each other via nodes and the entirety of FEs form a mesh. The elements can be of numerous dimension, like 1D elements as lines or beams, 2D elements as plates or 3D elements as tetrahedrons. A visual representation of these elements can be seen in Figures 1.2a, 1.2b and 1.2c. Additionally, the number of nodes assigned to one element can vary, leading to linear or nonlinear elements. Therefore, the displacement of a single node can be interpolated by a linear or a nonlinear shape function.[67] Together with the equilibrium equations, the strain-displacement relations and the constitutive equations, the displacement of each node is calculated. This relationship can be formulated as

$$\underline{\underline{K}}\,\underline{U} = \underline{F} \tag{1.1}$$

where $\underline{\underline{K}}$ is the symmetric element stiffness matrix which gives a relationship between the nodal displacements $\underline{U}$ and the nodal forces $\underline{F}$ and is calculated for each element. To obtain a response of the complete system, the global stiffness matrix is assembled, which gives a force displacement relationship for each node. Finally, the stresses and strains can be obtained by solving the governing equations. In conclusion, complex geometries and complicated loading cases can be solved by this discretization method.[10, 67]

(a)	(b)	(c)
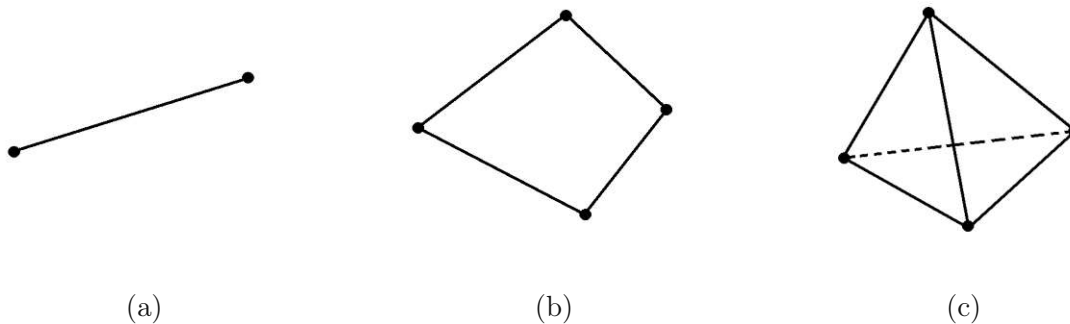
Figure 1.2: Representation of FE shapes (a) 1D line element (b) 2D plane element (c) 3D tetrahedral element

1.4.2 Topological Optimization

The area of TO is a scientific field which first started in the aerospace and automobile industry and got adopted by medical implant designers in the past few decades.[14, 15] TO offers an innovative approach for optimizing the mechanical properties of an implant by redesigning the material distribution in a specific domain.[15] This redesign relies upon the loading scenarios and BCs are subject to the objective function, which minimizes or maximizes a physical quantity.[15] An example for such a physical quantity is the mean compliance, that represents the inverse of the global stiffness. The FEM is used to discretize the design do-
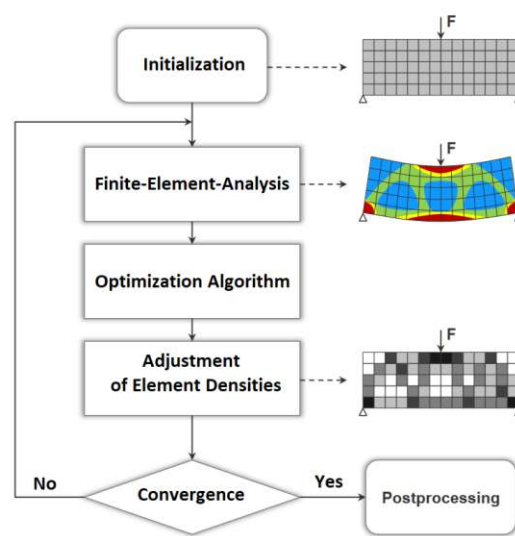
Figure 1.3: Iterative process of the SIMP-Method.[68]

main, whereupon the TO procedure determines whether the element in question has sufficient stress levels, if not, the element in question is removed to expand overall efficiency.[15] FEM software tools like *Hypermesh* (Altair Engineering, Troy, MI) can attain such optimization results. Typically, in implant design TO can be used for the global layout structure as well as for the local micro-structure.

From a theoretical point of view, the principle of a TO algorithm bares upon various methodologies, such as the variable density method, called solid isotropic material penalization (SIMP) model.[15] This method simply distributes material of a structure in a defined space upon the obtained stress results of the FE analysis.[69] In the SIMP approach, a so-called design variable x_i is assigned to each element, which consists of the material density $\rho_{i,0}$ of the solid element and the density ρ_i assigned to the element. The design variable represents the normalized density and is therefore in the range between 0 and 1 as seen in equation 1.2.

$$x_i = \frac{\rho_i}{\rho_{i,0}} \text{ with } 0 < x_i \leq 1 \tag{1.2}$$

The relationship between the design variable and the elements' elasticity is described by the Young's modulus E, as seen in equation 1.3, with $E_{i,0}$ being the Young's modulus of the starting material and E_i the reduced Young's modulus.

$$x_i^p = \frac{E_i}{E_{i,0}} \text{ with } p > 1 \tag{1.3}$$

The exponent p is the so called penalization exponent which greatly effects the optimization result. This coefficient leads to easier distinguishable results, since density values of 0,5 can be avoided.[68] Figure 1.3 gives a visualization of the iterative SIMP algorithm, which is stopped if no further improvement to the previous iteration is achieved, hence the optimization has converged.

For patient specific biomedical applications, TO is successfully implemented for arthorplasty, maxillofacial surgery, trauma surgery, spine surgery, and dentistry regarding mass reduction while maintaining its strength.[15, 16, 63, 70, 71]

1.5 Additive Manufacturing Technology

A single unit of a personalized implant can be fabricated by means of rapid prototyping (RP). RP describes a material AM process in which an object is created through layer-wise material deposition.[72] A CAD model is divided into numerous cross-sectional slices, which are assembled layer-by-layer by a 3D printer. This RP process has revolutionized the manufacturing process and significantly reduced costs and fabrication time for single item production or low-scale series.[72] Additionally, novel structures and geometries can be fabricated, which before were impossible by conventional manufacturing techniques.[15] This leads to the revision of already forgotten designs, such as the subperiosteal implant.[50] Ergo, the concept of RP can lead to a faster and enhanced treatment.[5]

The term AM formally describes the process of RP. Advancements in the output quality from these machines, however, manifest in a much stronger correlation to a final product as to a prototype.[73] Additionally, the term RP doesn't take the manufacturing principle into account, since all assembled parts are produced in a layer-wise fashion.[73] Therefore, a consensus between the majority of standards bodies around the globe has been found by adopting the term AM for a RP process.[73]
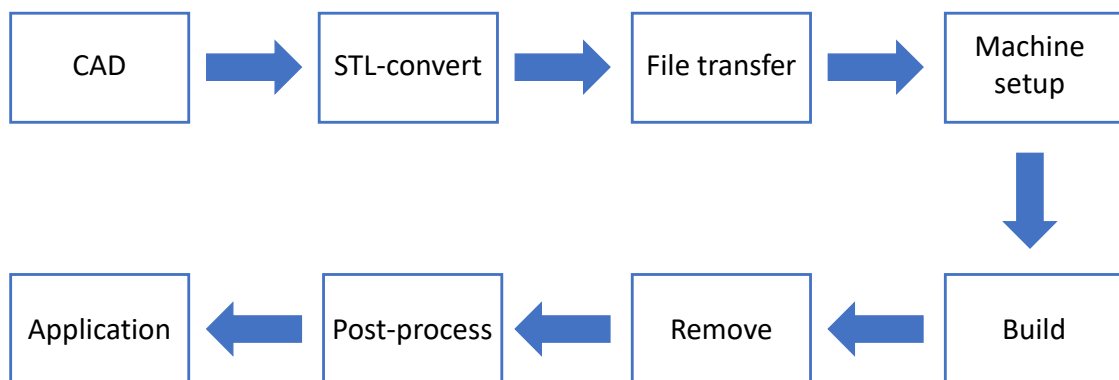
Figure 1.4: General AM workflow of CAD model to physical part in 8 stages.[73]

The basic principle of the AM technology is, that an element is built up by adding material in layers. Each layer represents a thin cross-section of the element, which is acquired from the element's 3D CAD model. By adjusting the layer height, the final product will be finer or coarser, implying that the AM approach leads to an approximation of the model.[73] Generally, the workflow of an AM process, as seen in figure 1.4, starts with a software model that defines the geometry of the part. This part is then converted into a Standard Triangle Language (STL) file format, which is then sent to a AM machine. After the machine building parameters like layer thickness, energy source, timings etc. are defined, the building process can be started. Once the AM machine finished the building job, the new part can

be removed and post-processed. This post-processing may include the removal of potential support structures, which are needed, e.g. for the building process of overhangs, cleaning or energy-treatments for enhancing the material properties. Finally, the part is now ready for use.[73]

As an example for biomedical applications, in dentistry, due to the necessity of customization, the AM technology has already successfully been utilized and lead to significant changes in the patients' treatments.[74, 75] Today, the 2 most prominent AM technologies in the field of dentistry are stereolithography (SLA), as example for the fabrication of aligners, and direct metal laser sintering (DMLS), for dental crowns and appliance frames.[76] The SLA process utilizes the photopolymerization technique, where light-sensitive, liquid resins inside a vat solidify at a specific wave length. Either a laser, as in the SLA process or a projector as in the digital light processing (DLP) process can be used. The area exposed to the light tempers and the next layer can be cured.[76, 77] The DMLS process utilizes a laser beam, which fuses a metal powder at a precise point, without melting.[73] The next layer of metal powder is then added to the building platform and so the part can be fabricated layer-by-layer.[76] Since this process is based on sintering, alloys which contain materials of various melting points, like the nylon and aluminium composite Alumide, can be employed.[73] This process is opposed by the selective laser melting (SLM) process, which also utilizes a laser beam, however fully melts a metal powder at a precise point. This results in well-bonded and high-density structures, yet higher energy levels are required to completely melt the metal powder and only one material per print is feasible.[73]

1.5.1 Additive Manufacturing of Ceramic Materials

Another group of materials currently used in dentistry are oxide-ceramics. The material Zirconia (ZrO_2) is already the standard material in implant dentistry for abutments, which provide the link between the prosthesis and the implant.[78] Due to their high biological compatibility and long-term durability in abutments, it is of interest to elucidate additional potential use cases, like the application as subperiosteal implants.

Ceramic oxide materials are either based on the oxide of a single element, as ZrO_2, or contain several cations of different elements (e.g. $MgAl_2O_4$, $BaTiO_3$, $ZnFe2O_4$) in their crystal lattice in addition to oxygen ions. These are then referred to as complex oxides or mixed oxides.[79] Due to it's bio-compatibility, excellent toughness and strength and white colour, ZrO_2 has developed into a multipurpose material in dentistry.[22] This excellent toughness and strength of ZrO_2 can be achieved by a special alloying strategy.[78] Therefore, rare earth oxides like Yttrium (Y_2O_3), CaO or MgO are added to ZrO_2 in order to stabilize the ZrO_2 in it's tetragonal phase at room temperature.[78, 79] Usually, ZrO_2 presents as a monoclinic

structure at room temperature. At about 1170°C it undergoes a phase transformation to the tetragonal crystal system and at around 2370°C ZrO_2 will transform to cubic.[80] The phase transformation form the monoclinic to the tetragonal phase is coupled to a volumetric shrinkage of approximately 3% as a result of the denser packing.[78] Hence, to stabilize the ZrO_2 in it's tetragonal phase is of great importance, since the possibility of a stress induced phase transformation from tetragonal to monoclinic arises, which is in the opposite way associated with an increase in volume. This increase in volume has the potential to lower the tensile stresses within the object, leading to higher tolerable external stresses.[78]

A possible technology which allows the AM process of an Y_2O_3-stabilized ZrO_2 object is the lithography-based ceramic manufacturing (LCM) technique.[81, 82] The LCM process is based on the DLP process, were a ceramic powder is dissolved in a photopolymeric resin. A light engine then cures the requested area and again builds the part in a layer-wise fashion. The result is a green part with low strength which is composed of the ceramic particles and an organic photopolymer. This green part then undergoes post-processing, which consists of debinding (removal of the photopolymeric matrix) and sintering.[81] Sintering is a heat treatment below the powder's absolute melting point over a specified period of time, which allows the particles to join together and form a dense body of high strength.[79]

1.5.2 Fracture of Ceramics

The understanding of stress concentrations, especially in long-bearing applications like implants, is essential.[73] Ceramics are mostly composed of ionic or covalent bonds, which induce high hardness and inherent brittleness at ambient temperatures, however, this causes that stress concentrations cannot be relaxed by plastic deformation.[83] In ceramics, fracture generally originates from small defects that represent discontinuities in the microstructure. The strength then relies on the size of the largest flaw in a component.[83] The fracture itself is caused by the principal tensile stresses in the component, producing a crack path almost perpendicular to the load direction.[83] Therefore, an overload may result into catastrophic failure.[83] This makes the need for biomechanical deliberations apparent.

Mechanical tests, however, are more difficult for ceramic materials than for ductile materials, as any malalignment of the test samples can lead to severe problems. These cannot be compensated by small amounts of plastic deformation, leading to the requirement of very sophisticated test setups.[83] Consequently, a FEA could serve as guide for finding stress concentrations leading to an enhanced design to reduce the need of mechanically testing several different specimens.

Additionally, in the AM process, several material issues, like porosity, delamination or cracks,

can arise, which, regarding the almost complete absence of plastic deformation in ceramics, should be addressed.[73, 83] Moreover, local thickness differences caused by material buildup could introduce stress concentrations in the sintering process, and therefore should be avoided.[73]

1.6 Research Question and Hypothesis

The aim of this thesis was to design and optimize a patient-specific subperiosteal implant. The implant is thought to be made out of a Yttrium-stabilized Zircon oxide by utilizing TO for assigning lattice in potential areas of the implant. Real patient image data with present pathologies was utilized under physiological loading conditions. Since the implant should incorporate a lattice structure to promote osseointegration, the method of TO was used to define areas for potential sites where a lattice may be added. Hence, this thesis addressed the question if a Yttrium-stabilized Zircon oxide can be implemented for the design of subperiosteal implants for edentulous patients. Furthermore, it was investigated if the method of TO can comprehensibly be utilized for deciding the locations of an osseointegration promoting lattice?

2 Initial Design and Optimization of the Implant

The design process was performed in 5 steps, as seen in figure 2.1, and consisted of 2 models, an initial model without topological optimization and a redesigned model that was evaluated according to the same boundary conditions and loading cases as the initial model taking into account the results of TO. Both models were meshed for the simulation in order to achieve high quality results with perfect bonding between all different parts. Following image segmentation from an anonymized patient's CT, an initial implant design matching the patient's anatomy was performed using *Materialise 3-matic 15.0*. The second step was the preparation of the implant to fulfill perfect bonding between mesh elements in *Materialise 3-matic 15.0* together with *Autodesk Meshmixer 3.5*. The third step was the TO process and FE simulation with *Altair HyperWorks 2021 Student Edition* and the fourth step was the redesign of the implant with *Materialise 3-matic 15.0* and *Autodesk Meshmixer 3.5*. Finally, the fifth and final step was the numerical evaluation of stress fields using FE simulation with *Altair HyperWorks 2021 Student Edition*. Any software commands specified in this thesis are indicated by the `typewriter` font.
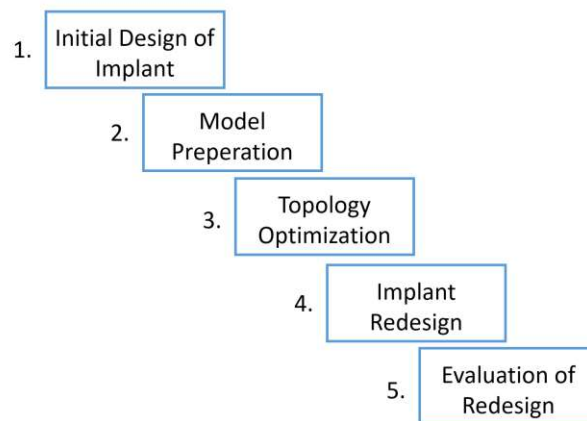
Figure 2.1: Flowchart of the 5 step workflow utilized in this thesis.

17

2.1 Initial Design of the Subperiosteal Implant

Generally, the treatment plan for an implant starts with the patient's medical history, as comorbidities or specific patient conditions can alter the biomechanical and environmental stresses of the pathological region of interest.[84] Implant design might be influenced by knowing if the patient is a smoker, has diabetes or any pathological occlusion like clenching (maximum pressing or clamping of the teeth) or bruxism (involuntary grinding of the teeth).[85] If any of these diseases occur, this must be tackled beforehand, since e.g. smoking vastly alters the desired outcome of the treatment and is associated with higher failure rates and complications.[86] Pathological occlusion mechanisms like bruxism or clenching will lead to early implant failure.[87] Following the diagnostics of the patient's medical history, the patient's medical images, e.g. via CT imaging, are interpreted regarding bone quality and quantity. Additionally, the surrounding soft tissue such as lip profile is of importance, given the fact that implants are designed in consistence with the prosthesis to avoid significant impairment of the facial aesthetics.[88]

In this thesis, the used patient's medical data was anonymized, and the medical history was supposed not to lead to contraindications to an implant, implying that the analysis of the medical images could be initiated. The CT scan was performed with settings indicated in table 2.1. A segmentation dataset of bone was available (having being previously performed by thesholding using the *Materialise Mimics Innovation Suite* software).

Modality	CT (Siemens, Erlangen, Germany)
Model Name	SOMATOM Force
Software version	Syngo CT VB20A
Slice thickness	0,6 mm
Kilovoltage peak (kVp)	100 kV
Exposure time	500 s
X-ray tube current	37 mA
Pixel spacing	0,43 mm x 0,43 mm
Date	31.05.2021

Table 2.1: CT settings.

The segmented bone *.stl file could be opened with *Materialise 3-matic 15.0* as shown in figure 2.2. In this picture, the skull including the maxilla and the mandibula and a part of the spine of the patient can be seen.

Additionally, on top of the mandibula, fragments of prior implants can be identified. For the placement and orientation of the abutments it is necessary to find the occlusion plane (OP) together with the lip plane (LP). The LP is a guidance plane, which is oriented according

Figure 2.2: Maxilla and mandibula of the patient including the skull opened in *Materialise 3-matic 15.0*

to the profile of the lips. According to Sato et al. 2007, the OP is tilted 6,8°±4°about the frontal axis, parallel to the Frankfort horizontal (FH) plane and translated according to the positions of the mandibula and the lips.[89] To horizontally adjust the skull, the FH plane is needed. It is defined via craniometric points on the skull, in order that the FH plane passes through the most superior and outer point of the external auditory meatus, which is also called the Porion point, and through the inferior border of the orbitale.[90] The FH-plane including the craniometric points marked in yellow can be seen in figure 2.3.

Subsequently, the OP can be found and adjusted together with the patient's lip profile. The OP together with a section of the patient's soft tissue can be seen in figure 2.4a. Next, the LP is needed for the orientation of the abutments[88], which can be seen in figure 2.4b.

To design the maxilla implant, the bone's surface needs to be refined and a smaller region of interest can be considered, since not the whole skull and the spine is needed for the subsequent design process. The refinement can be done via `Remesh → Quality Preserving Reduce Triangles` and the regions which are not needed can be cut via `Finish → Trim`. The result can be seen in figure 2.5.
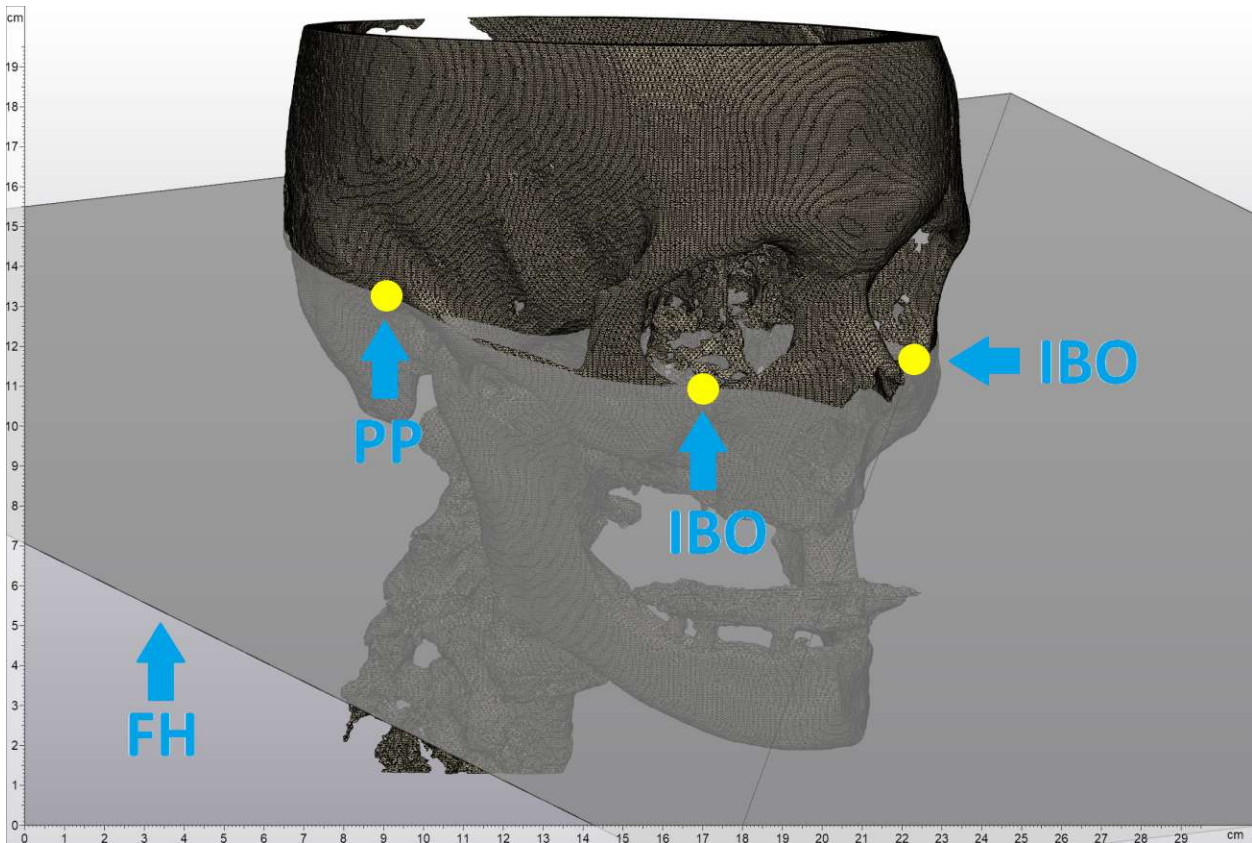
Figure 2.3: Patient's skull including the FH-plane. FH-plane is passing through the Porion Point (PP), which is defined by the most superior and outer point of the external auditory meatus, and the inferior border of the orbitale (IBO).

(a)   (b)
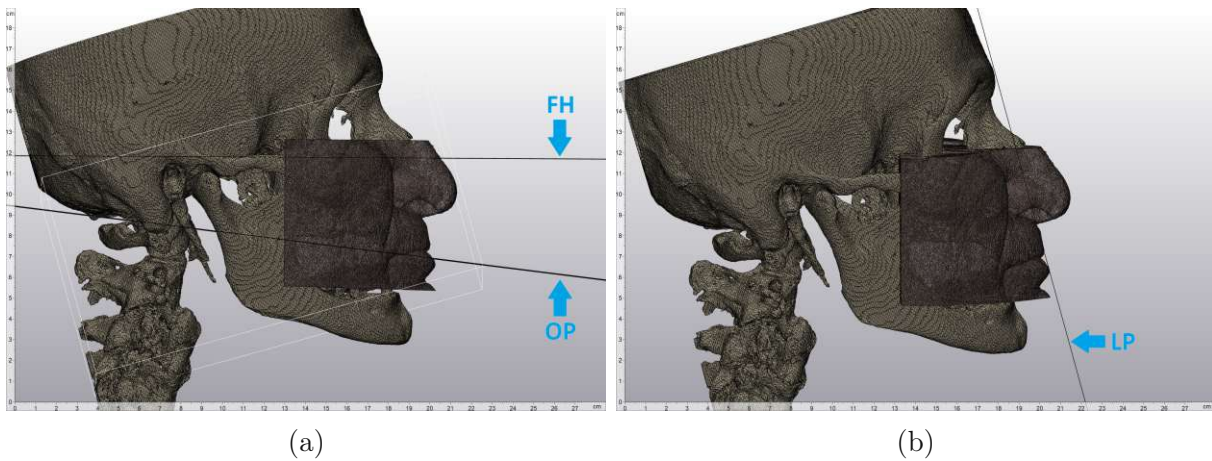
Figure 2.4: (a) Patient's skull including a section of the patient's soft tissue, the FH-plane and the OP. The OP is adjusted according to the patient's lips (b) Patient's skull including a section of the patient's soft tissue and the LP.

A prerequisite for the implant design was that an osseointegration promoting material can be applied to the bone facing part of the implant. Therefore, a 0,5 mm uniform gap, accounting for this other material between the implant and the maxilla has to be adapted. So, for the design of the implant the bone is enlarged by a 0,5 mm uniform offset via `Design → Offset`

Figure 2.5: Remeshed and trimmed skull

(a)   (b)
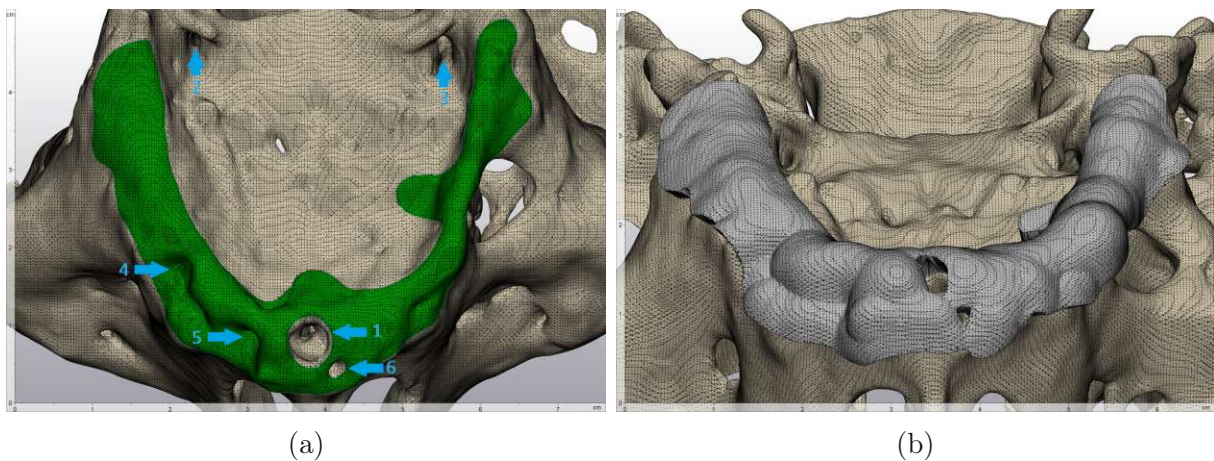
Figure 2.6: (a) Inferior view of the border of the maxillary implant in green with marked regions, in which 1, 2 and 3 are relief areas, which must not be loaded. 1: fossa incisiva; 2: foramen palatinum majus sinister; 3: foramen palatinum majus dexter; 4,5 and 6: pathological valleys of unknown origin. The green surface was used for the implant extrusion (b) Anterior inferior view of extruded border of the maxillary implant by 2,5 mm

$\rightarrow$ `Uniform Offset`. Now the border of the implant can be drawn via `Curve` $\rightarrow$ `Create Curve`. This function allows to draw a smooth curve that is attached to the bone's surface. As already mentioned, the maxilla consists of stress and relief areas, meaning, areas which

can be loaded and areas that must not be loaded. So, the implant's border is drawn according to these stress and relief areas. The border can be seen in figure 2.6a.

Number 1 in figure 2.6a marks the fossa incisiva, which is an anatomical region and the opening of the canalis incisivus posterior to the incisors that gives passage for a vascular nerve cord. The foramina palatina majoria, marked with numbers 2 and 3, give way for the passing of the descending palatine vessels and greater palatine nerve. The numbers 4, 5 and 6 mark regions of pathological valleys of unknown origin(possible prior implant locations), with the difference to 1,2 and 3 that these regions may be loaded. Hence, the border area can be copied and separated to a new part and then extruded across 2,5 mm via the function `Design → Offset → Uniform Offset`.

In figure 2.6b, the bone and the extruded border as new part can be seen from an anterior inferior perspective. The part still has sharp edges which need to be smoothened. Additionally, the surface has many valleys, which are undesired. So, to create a smooth surface, guiding lines were added with which a new surface was built. Thus, the rough surface was deleted and the new built surface was added to the part. A close-up section of the part before and after the described operation can be seen in figures 2.7a and 2.7b.

Thereafter, 6 abutments, which carry the actual dental prosthesis, each with a geometry shown in figure 2.8a, were added according to predefined locations on the maxilla. The abutments were aligned according to the LP and the OP, which can be seen in figure 2.8b. There you can see the implant from a medial view with an offsetted LP and OP in order to visualize the alignment of the abutments.

The implant is supposed to be mounted onto the bone via two 2 mm titanium screws. Hence, two screw holes were added and the implant's surface around the screw holes were flattened.

The implant's design process was performed together with physicians, who described the implant requirements and evaluated iteratively the implant's design. As an example for this iterative process, the implant's medial protrusion, as marked by an arrow in figure 2.9a, was found to be unprofitable since it may introduce stress onto the sutura palatina mediana, which is undesired. So, the implant was altered according to this considerations. The implant in the exact position on the maxilla can be seen from an inferior view in figure 2.9b and isolated in figure 2.10.
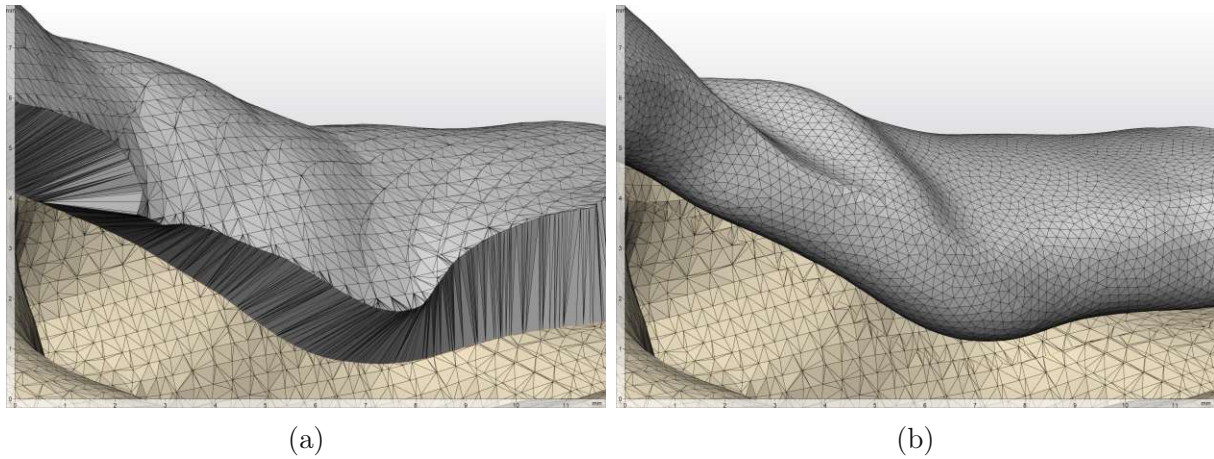
Figure 2.7: Section of the implant to visualize the smooth surface and border with a triangle edge length of 0,2 mm, (a) before smoothing, and (b) after smoothing.
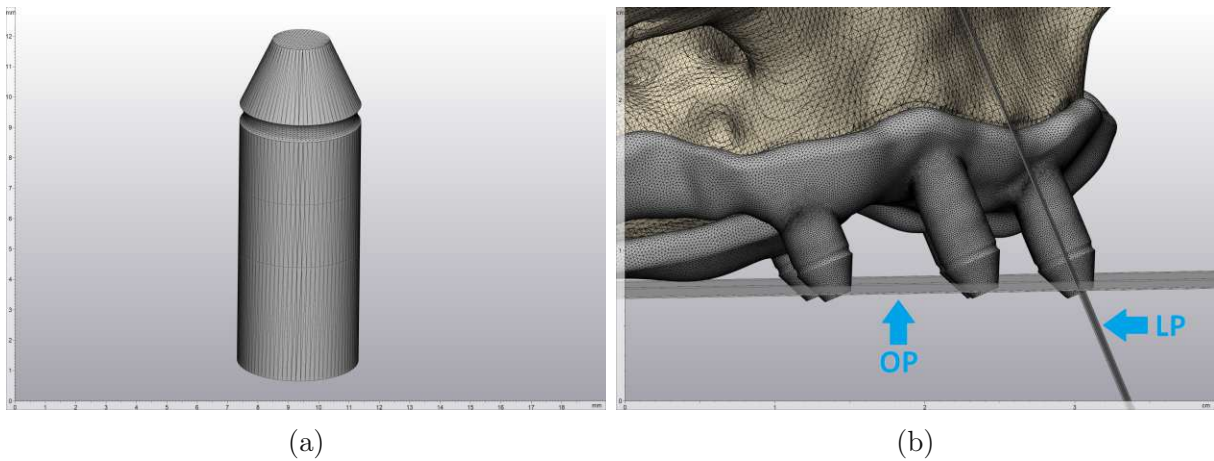
Figure 2.8: (a) Isolated abutment with the caudal surface at the top. (b) Medial view of a section of the implant with an offsetted LP towards the abutments and an offsetted OP to visualize the alignment of the abutments.
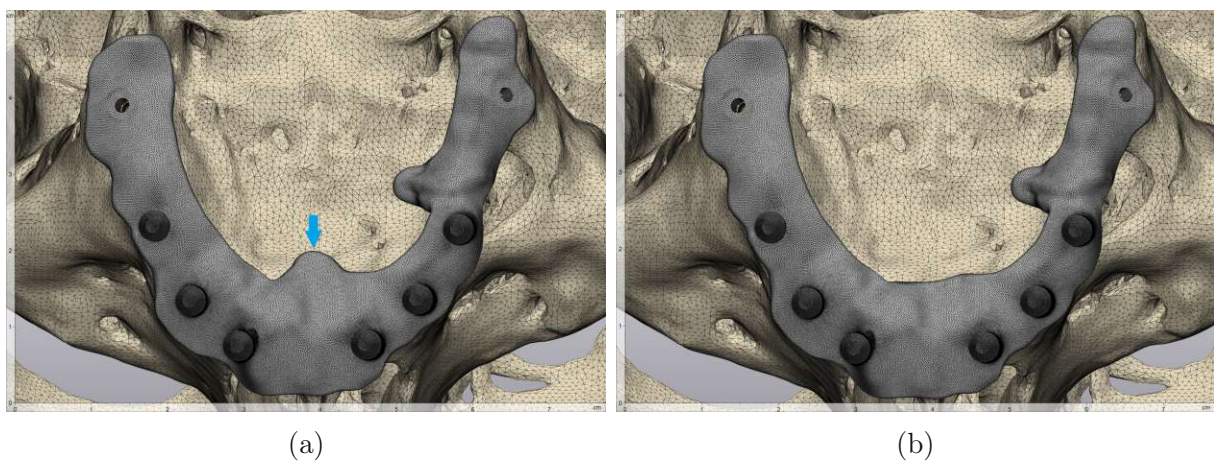
Figure 2.9: (a) Inferior view of the implant with an arrow which marks a medial protrusion that should be avoided and (b) the final implant without the protrusion.
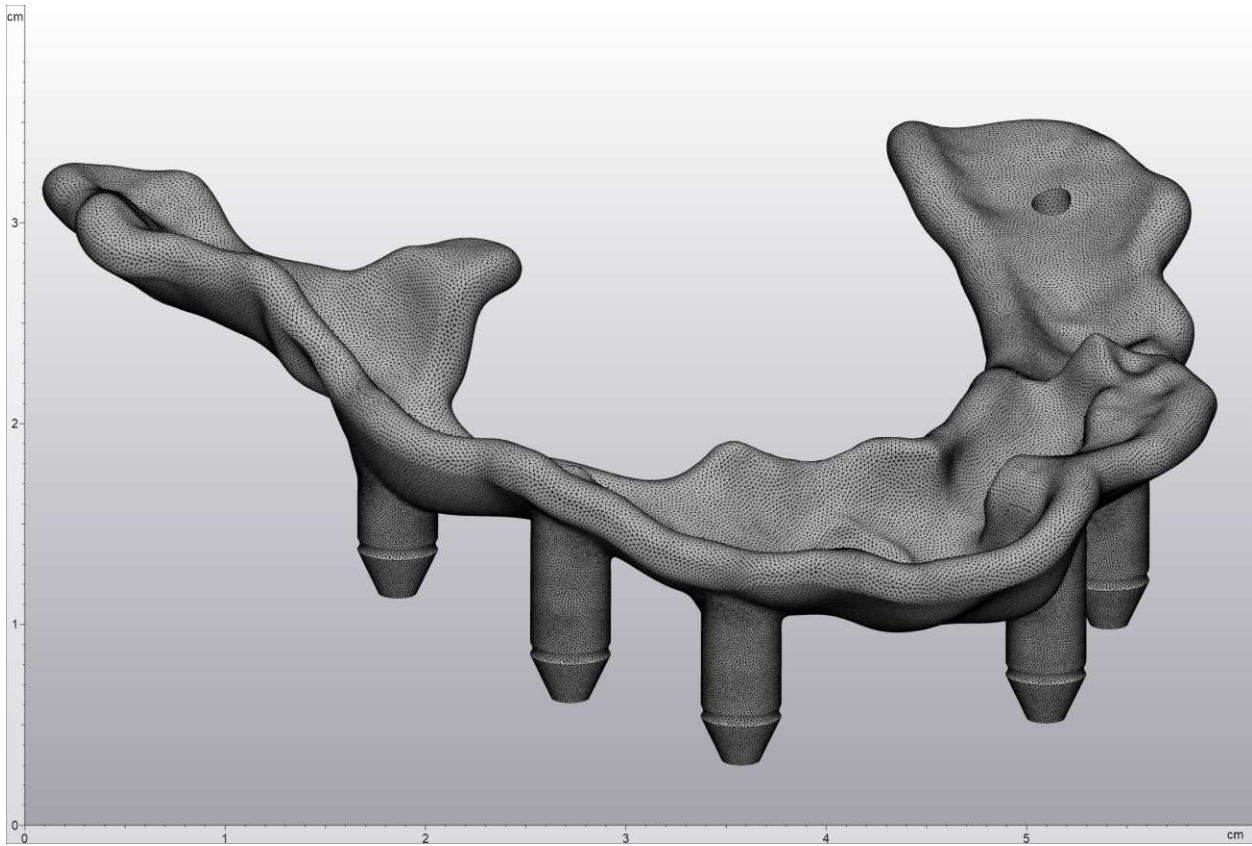
Figure 2.10: The implant used for the optimization.

2.2 Model Preparation

The material used for the implant is a Yttrium-stabilized Zircon oxide, named LithaCon 3Y 210 (Lithoz GmbH, Vienna, Austria). A design prerequisite for the additive manufacturing of this ceramic material is to avoid large bulk material accumulations, which could lead to failure in the manufacturing post processing.[91] Additionally, osseointegration would be facilitated by a lattice structure.[19] Therefore, a topological optimization was proposed to find implante regions that allow a lattice structure geometry, implicitly leading to a reduction of material accumulation.

The individual parts need to be prepared for the FE analysis in order to obtain a perfect bonding between all components. This means all components have a perfect node to node connection, that allows a linear FE analysis. Otherwise, the concept of contact needs to be addressed which would lead to a kinematic nonlinearity, thus if possible, it should be avoided due to increasing computational complexity and time.[92] These alterations were performed with *Materialise 3-matic 15.0* if not stated differently.

First, the bone's area of interest was further narrowed via `Finish → Trim`, since not every part of the bone is needed for the FE simulation. Then, the bone and the implant were remeshed with a 1 mm triangle edge length and the option Preserve Surface Contours was active. Two 2 mm screw elements were added to the model and via `Design → Boolean Subtraction` the screw holes in the bone appended. Next, the component of the osseointegration layer is built, which was done by filling the 0,5 mm large space between the implant's and the bone's surface. In building this additional layer, 2 levels of osseointegration were simulated, one for complete osseointegration (100%) and one for partial osseointegration (30%). This was done by adjusting the Young's modulus of the layer according to the percentage of the total bone's Young's modulus. To build this part, the maxillary surface and the implant's contact surface were marked by `Mark → Triangle`, separated to a new part and then in *Meshmixer* closed to a single shell. The osseointegration layer can be seen in figure 2.11a. Via the command `Boolean Subtraction` perfect bonding accompanied by a uniform mesh cannot be established, therefore, the screws' used for the FE analysis needed to be built via the surfaces of the adjacent parts, which were the implant, the osseointegration layer and the bone. Analogous to building the osseointegration layer, the triangles building up the screw holes of the individual parts were marked, separated to a new part, normals inverted and merged to a single, closed surface. A screw modeled after this workflow can be seen in figure 2.11b.

(a)   (b)
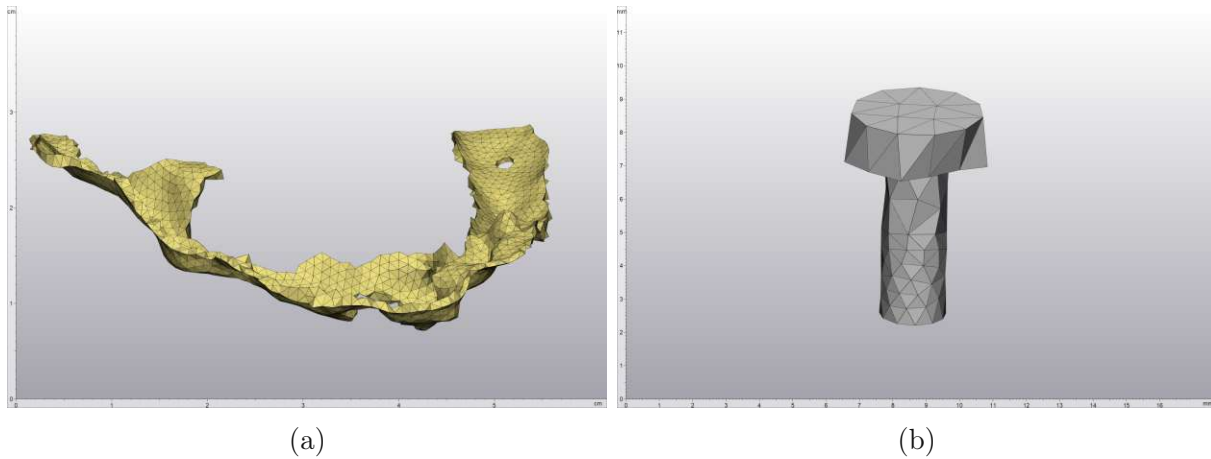
Figure 2.11: (a) 0,5 mm thick osseointegration layer and (b) screw prepared for the FE analysis, with 1 mm triangle edge length.

Finally, a 4 node tetrahedron volume mesh via `Remesh → Create Volume Mesh` can be created and the components can be exported as *.FEM files. The model assembly with all participating components are displayed in figure 2.12.
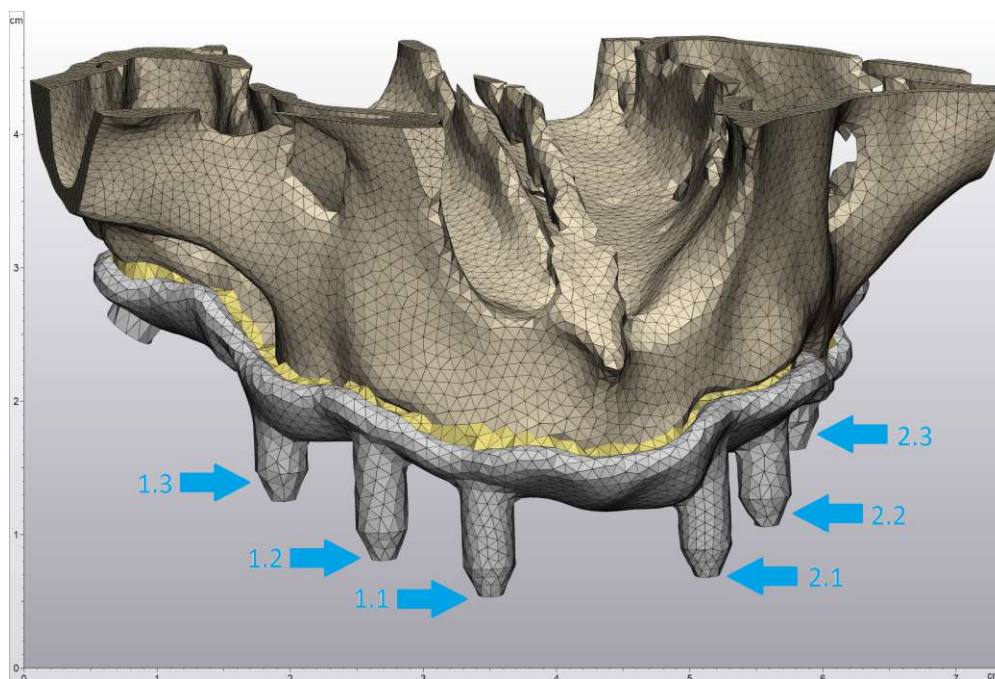
Figure 2.12: Model with individual components: the maxilla in the colour beige, the osseointegration layer in yellow, the implant in grey, the screws in grey. Additionally, the abutments were marked with numbers.

2.3 Topology Optimization

The *.FEM files of the components can now be imported into *Altair HyperWorks 2021 Student Edition* with the implemented reader *OptiStruct*. All parts were imported with 0 errors. First, perfect bonding between the all components was established by the command `Faces → Find Equivalence`. This command connects meshes by merging coincident nodes. 2597 equivalent nodes were found and equalised. These nodes highlighted on the cranial part of the implant can be seen in figure 2.13a.

(a)   (b)
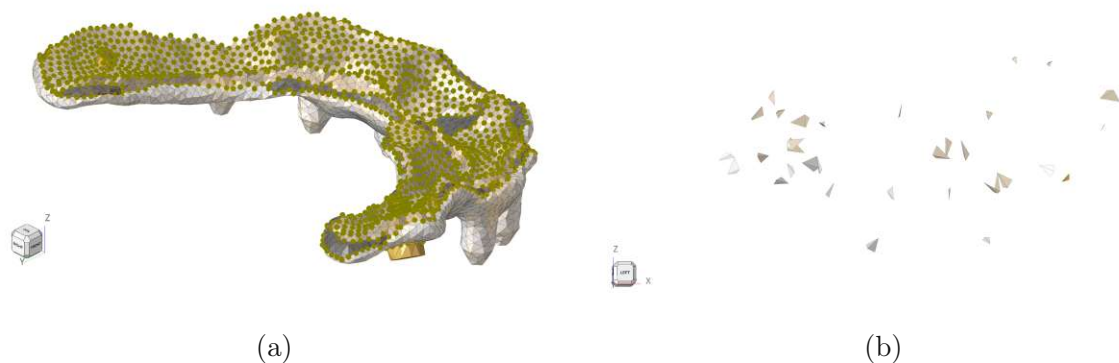
Figure 2.13: (a) 2597 marked equivalent nodes between the bone, the implant, the osseointegration layer and the screws (b) Visualization of the elements, which failed the `tet collapse` command.

To improve the tetrahedral element quality, the `tet collapse` value of all elements can be checked and compared to a preset threshold value via `Tool → Check Element Quality`. This threshold value was chosen according to the *Altair HyperWorks* software manual and set to 0,1.[93] This value is computed for each tetrahedron 4 times. It is calculated by the distance from each of the four nodes of a tetrahedron to the opposite surface of each node. These 4 resulting distances are then divided by the square root of the surface area of their opposite side respectively. The minimal value obtained is normalize and output. This value is 1 for a perfect tetrahedron and diverges to 0 for a totally collapsed element.[93] Here, 35 elements were marked as to be below the threshold value of 0,1. These elements can be seen in figure 2.13b. These elements need to be remeshed in order to improve the model. Therefore, the tetrahedrons next to these elements were displayed via `Find → Adjacent Elements`. Then the failed elements together with the adjacent elements were remeshed via the command `3D → Remesh → Tetra Remesh`. The subsequent element quality check showed all elements were above the threshold value of 0,1. The mesh can be seen as acceptable and ready for the simulation. A list of the mesh properties are listed in table 2.2, with the components implant design and implant non-design are explained later in this thesis.

Component	Nodes	Elements
Bone	64335	360535
Implant Design	12478	65914
Implant Non-Design	2274	9767
Osseointegration layer	2455	6716
Screw right	150	500
Screw left	94	278

Table 2.2: FE mesh properties used for the simulation.

Thereafter, the linear elastic, isotropic material properties were assigned and the values are recorded in table 2.3. The Young's modulus of compact bone is in the range of 13,7 to 14,8 GPa and trabecular bone of 1,85 to 7,9 GPa.[94, 95] Here, the maxilla was assumed to be of uniform bone throughout of 9 GPa, which is in the range of present literature.[96] Then, 6 rigid body elements (RBEs) at the caudal surface of each abutment were defined. The RBE function is used to define a reference node by linking the degree of freedom (DOF) of two or more nodes together. These reference nodes will serve later as the load application points at each abutment.

Component	Young's Modulus in GPa	Ultimate Strength in MPa	Poisson's Ratio
Bone	9	200 [97]	0,3 [96]
Implant LithaCon 3Y 210	205 [98]	940 [98]	0,31 [99]
Osseointegration 30%	2,7		0,3
Osseointegration 100%	9		0,3
Screw TiAl6V4	111 [87]	1000 [100]	0,34 [87]

Table 2.3: Material properties used for the finite element simulation.

Conditions at the boundary of the computational domain has to be specified in terms of assigned displacement and/or forces. In this thesis, two different boundary condition approaches for gathering the resulting stresses in the implant could have been taken. One approach is to obtain the occurring forces during mastication via the possible forces that jaw muscles can generate, or the other way would be to use measured biting forces. Since there is no consensus in the literature about the magnitude of the muscle forces, the path of using measured biting forces was adopted.[101–113]

Hence, four load collectors, which collect and organize loads, were defined. One for the single point constraints (SPCs), which restricts the movement of chosen nodes, and three for the loading scenarios, which are listed in table 2.4. Literature also presents great variation in the occlusion forces, therefore an average value during physiological mastication was chosen.[4, 16, 18, 87, 114–118] The loading scenarios should reproduce three individual chewing locations. One, referred to as molar right, which applies a force of 225 N on the reference node of abutment 1.2 and 1.3 corresponding to the patient chewing on the right

side. One, loading case incisor, which applies a force of 150 N on the reference node of abutment 1.1 and 2.1. The third loading scenario is called molar left, there a force of 225 N acts on the reference node of abutment 2.2 and 2.3. The orientation of the force vector perpendicular to the OP, lead to a force vector as seen in equation 2.1.

Abutment Load Step	1.1	1.2	1.3	2.1	2.2	2.3
Molar Right	0	225	225	0	0	0
Incisor	150	0	0	150	0	0
Molar Left	0	0	0	0	225	225

Table 2.4: Force magnitudes in N for each load step applied to each abutment in the direction of the force vector seen in equation 2.1 (abutment numbers according to figure 2.12). The force application point for each abutment is a reference node built of a RBE for each abutment.

$$\underline{f} = \begin{bmatrix} -0,0699 \\ -0,3844 \\ 0,9205 \end{bmatrix} \tag{2.1}$$
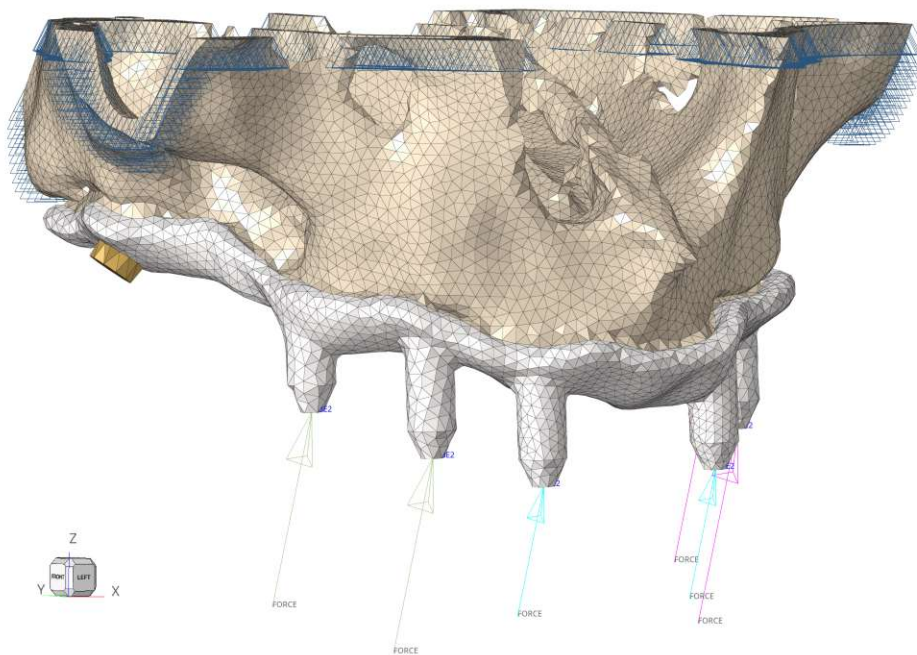
Figure 2.14: Visualization of the model in *Altair HyperWorks 2021*. Force vectors in the direction perpendicular to the OP. Green: molar right, abutment 1.2 and 1.3; teal: incisor, abutment 1.1 and 2.1; pink: molar left, abutment 2.2 and 2.3.

Figure 2.14 gives a visual representation of the FE model. The image shows the individual components, the SPCs as blue triangles on top and on the side of the bone and the 6 parallel force vectors. With these loading scenarios, 3 linear static load steps at 2 levels of osseointegration were simulated.

A prerequisite and unchangeable requirement for the implant were the abutments' and screw holes' locations and geometries. Therefore, the abutments and some elements adjacent to the screw holes were split from the original component via `Tool → Organize` to a new implant component, called Implant Non-Design, whereas the rest of the implant is called Implant Design. The implant non-design component cannot be altered by the TO solver and the implant design component can be. That new non-design component was addressed with the same material parameters as the original implant component.

A stress constraint, which gives the solver the BC of an element cannot overshoot a defined threshold stress value, was considered. This was set to 235 MPa, with the consideration of the ultimate strength of the material being 940 MPa, leading to a safety factor of 4.[98] Finally, two optimization responses, one constraint and one objective were defined. For the optimization responses, a volume fraction response type applied to the implant design region and a compliance response type for the whole model was chosen. The optimization constraint was connected to the volume fraction response type with an upper bound option of 30%, meaning only 30% of the material should remain. The objective was to minimize the compliance and each load step was calculated individually. All required parameters were defined and the optimization was initiated.

2.3.1 Results of the Optimization

The optimization was run 6 times with *OptiStruct*, twice for each load step, one for 30% osseointegration and one for 100% osseointegration. The solver spatially distributed material corresponding to the objective. This can be seen in figures 2.15, 2.16 and 2.17, which display different perspectives of the contour plot of the final iteration in *HyperView*. Each of these figures are built up in the same way. In the upper row the results with 100% osseointegration and in the lower row the 30% osseointegration results were depicted, in the left column the loading case molar right, in the middle column the incisor and in the right column the molar left loading case. As the contour plots graphically visualize the optimization results, they indicate the elements' density with different colours. Additionally, a certain threshold value can be set to exclude elements of lower density, leading to so called iso surfaces. These iso surfaces with a threshold value of 80% are displayed in figures 2.18, 2.19 and 2.20, meaning only elements with at least 80% element density are visible. Finally, these iso surfaces were extracted and exported as *.stl files.
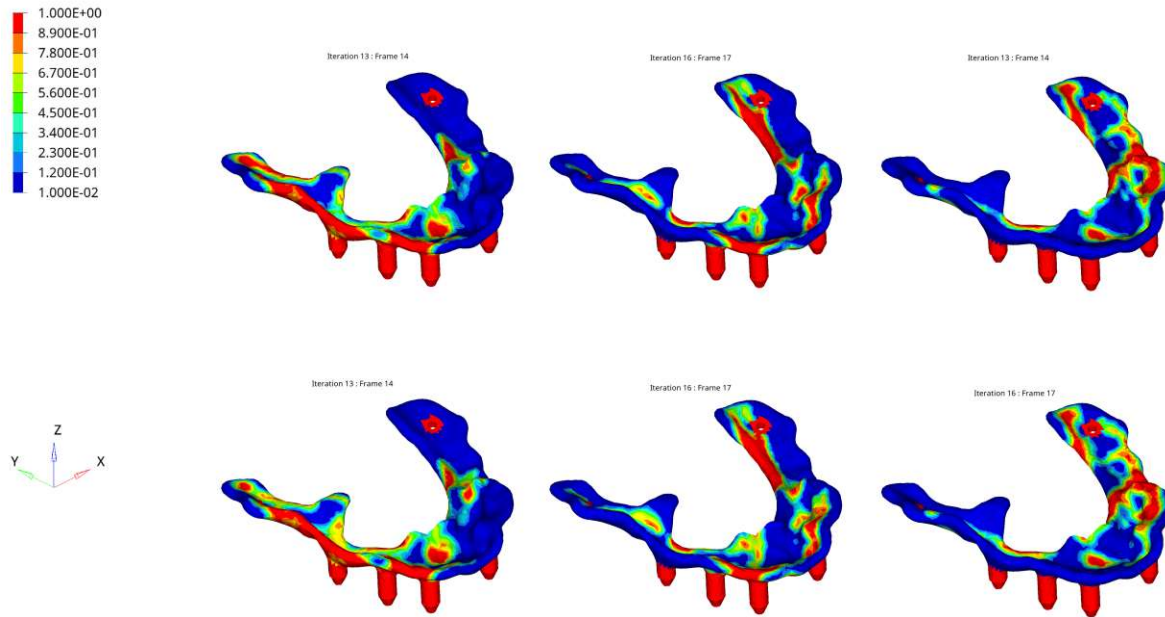
Figure 2.15: Isometric view of the results, colors indicate the calculated element density. In the upper row the different load cases with an osseointegration layer of 100%, starting with the molar right load case on the top left, the incisor load case in the middle and the molar left load case on the top right. In the lower row the corresponding images with an osseointegration shell of 30% Young's modulus of bone are visualized.
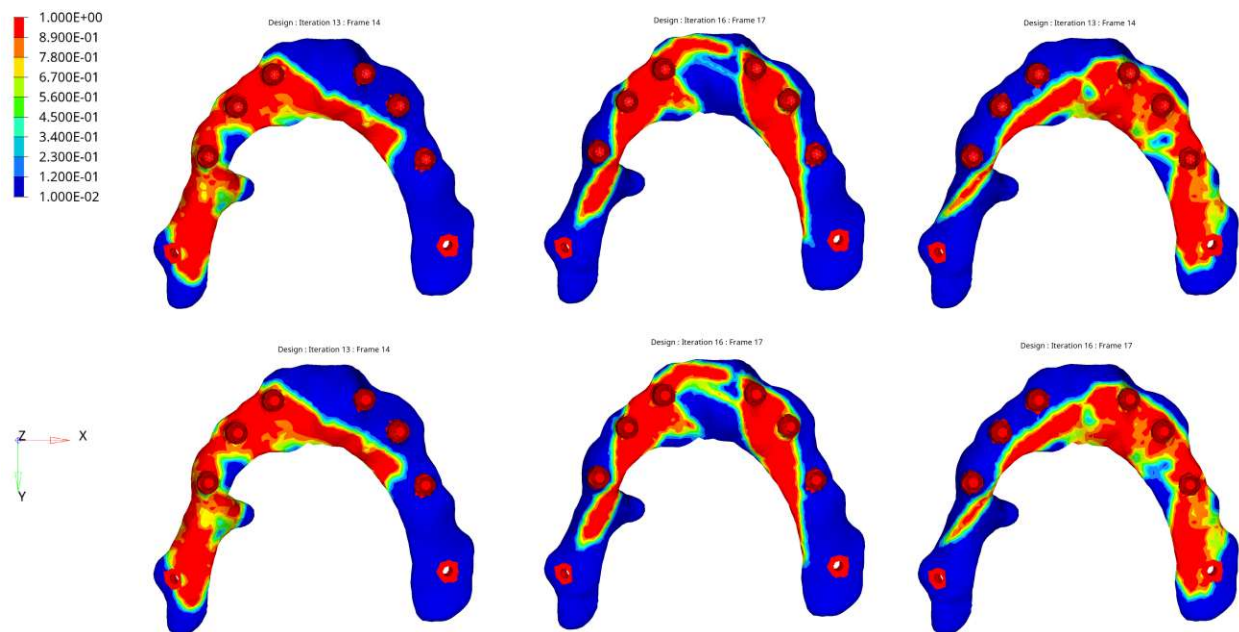
Figure 2.16: Bottom view of the results, colors indicate the calculated element density. In the upper row you can see the different load cases with an osseointegration shell of 100%, starting with the molar right load case on the top left, the incisor load case in the middle and the molar left load case on the top right. In the lower row you can see the corresponding images with an osseointegration shell of 30% Young's modulus of bone.
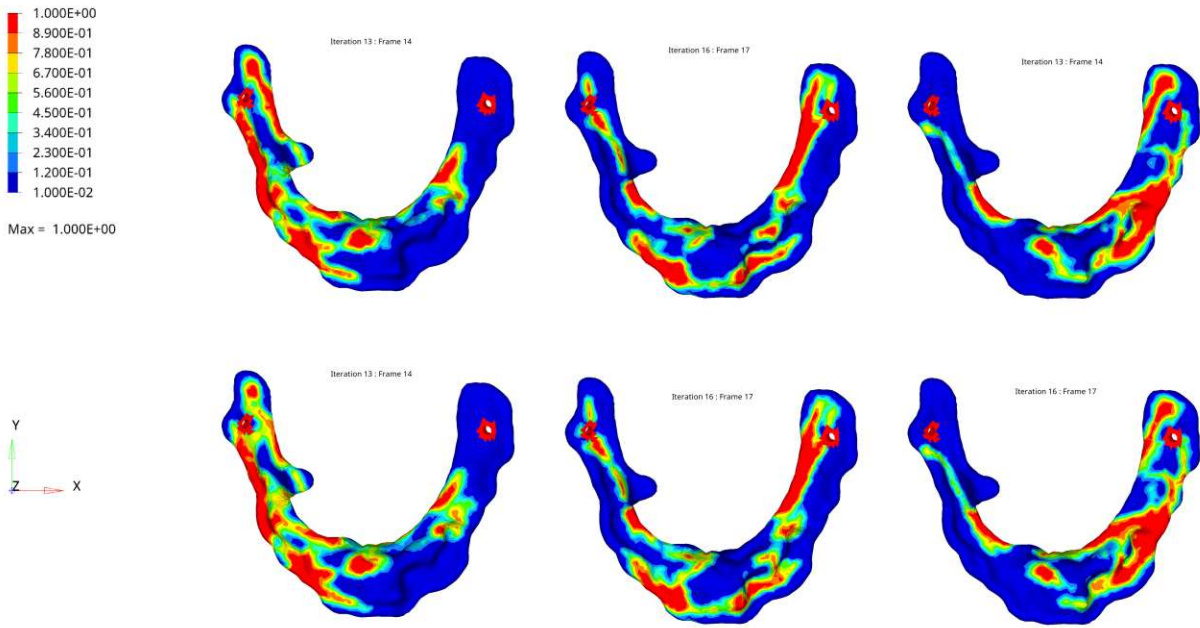
Figure 2.17: Top view of the results, colors indicate the calculated element density. In the upper row you can see the different load cases with an osseointegration shell of 100%, starting with the molar right load case on the top left, the incisor load case in the middle and the molar left load case on the top right. In the lower row you can see the corresponding images with an osseointegration shell of 30% Young's modulus of bone.
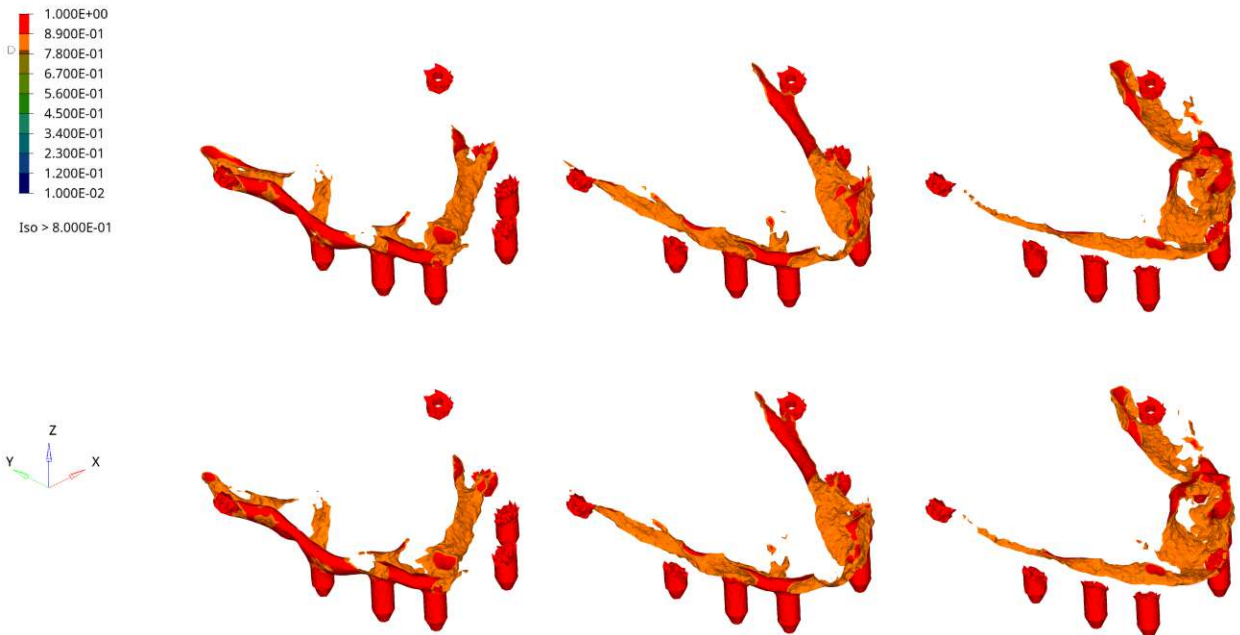
Figure 2.18: Isometric view of the iso surfaces, colors indicate the calculated element density.
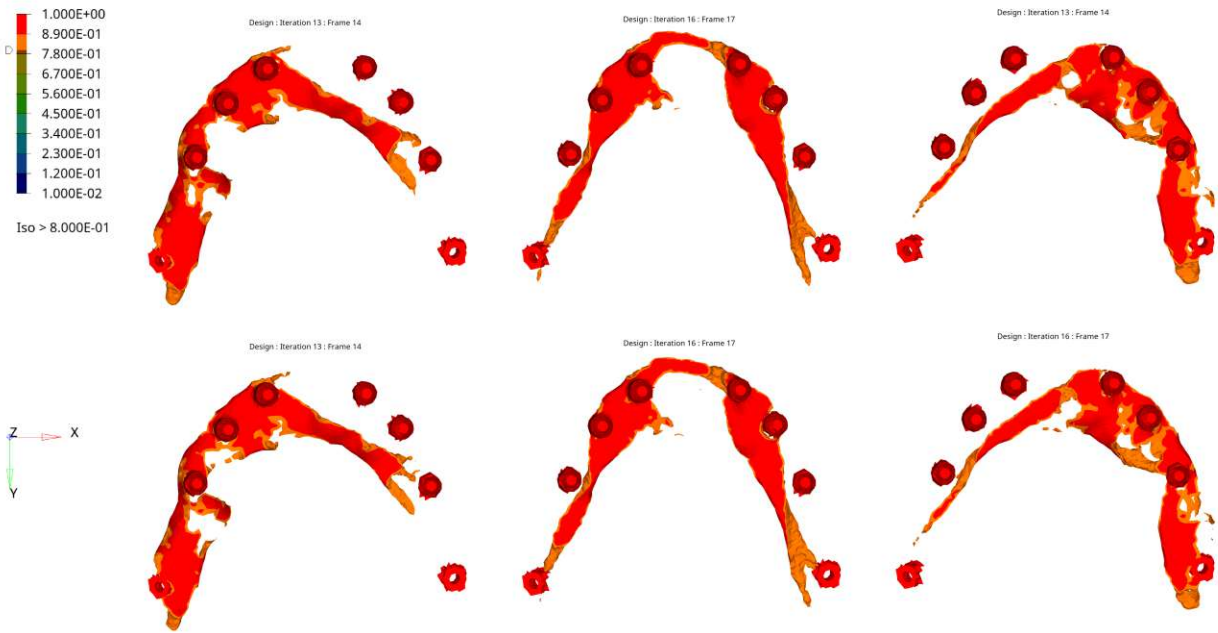
Figure 2.19: Bottom view of the iso surfaces, colors indicate the calculated element density.
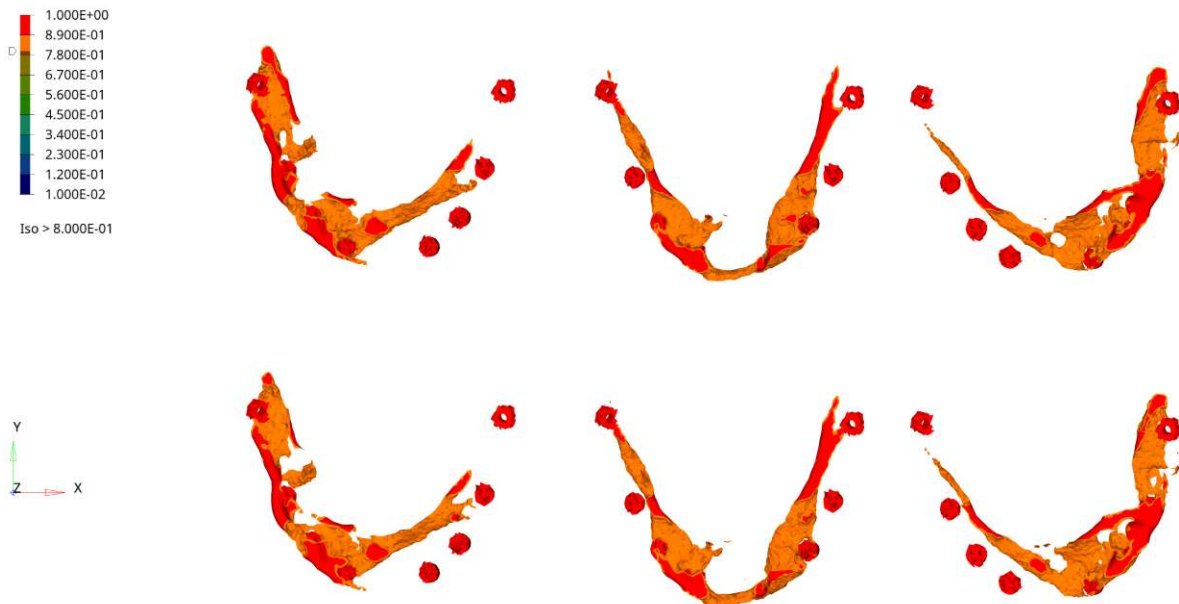
Figure 2.20: Top view of the iso surfaces, colors indicate the calculated element density.

2.3.2 Analysis and Considerations

The contour plots in figures 2.15, 2.16 and 2.17 show the material distribution results over the implant. The contrast between the results in the top row to the bottom row was hardly distinguishable, leading to the interpretation that the difference between the 30% and the 100% osseointegration layer was only marginal. As the thickness of the osseointegration layer is only 0,5 mm, the minor variation in the simulation results were reasonable.

The loading case molar right in figure 2.16 lead to an increased element density on the right wing of the implant directed towards the right titanium screw. Additionally, a beam like area of increased element density in the middle originating around the abutment 1.1 towards the abutment 2.3 was identifiable. The screws have a higher Young's modulus than the bone, therefore, they will absorb loads, so, the result is plausible.

The loading case incisors lead to a contour with elements of high density originate from abutments 1.1 and 2.1 and lead towards the screws. Analogous to previous argumentation, the result was justifiable.

In the loading case molar left, the solver suggested high dense elements around the loaded abutments 2.2 and 2.3 continuing towards the screws. Since the implant was asymmetrical, the outcome between the loading case molar right and molar left were asymmetrical.

A significant difference between the top and the bottom view in all loading scenarios was distinguishable. The solver proposed more material for areas adjacent to the peristeum, which was favorable for the intended bone augmentation design with an osseointegration promoting lattice structure at the implant-bone interface.

Since the abutments and the area around the screw holes were defined as non-design regions, the solver did not reduce the density from the maximum. Nevertheless, since it is advantageous for the manufacturing process to design hollow abutments in order to reduce possible temperature stresses during sintering, this was taken into account in the redesign step.

3 Implant Redesign and Evaluation of Redesign

This chapter addresses the fourth and fifth step in the design process, as depicted in figure 2.1. To redesign the implant, the iso surfaces of the individual load scenarios of the 100% osseointegration model with a threshold value of 0,8 were extracted and together with the initial implant model imported into *Autodesk Meshmixer 3.5*. Then, the iso surfaces were merged and used as template for the redesign. The merged iso plots are visible in figure 3.1. The merged iso plots together with the initial implant is shown in figure 3.2, with the iso surfaces in turquoise and the initial model in grey color.

The surface of the initial model was duplicated and an offset of 0,5 mm towards the inside of the implant applied followed by inverting the surface shell to build an implant with uniform thickness of 0,5 mm, which is feasible to manufacture by the 3D-printer with a tolerance of 0,1 mm. Next, the model was split horizontally in half into a top and bottom part. The bottom part was used for the redesign process. This part is in contact with the periosteum and needs to be a closed uniform surface to reduce blood accumulation or possibilities of infection after surgery. Therefore, the implant was redesigned by adding material to the inner surface of the bottom part via `Sculpt → Brushes`, so the redesigned implant would match the iso surface template. The redesigned model can be seen in figure 3.3.

The final step was to add a lattice structure to the model. Since the volume of the implant should stay the same, the whole initial implant was converted into lattice and then combined with the rebuilt model. This should ensure that the redesigned implant still has a curvature at its cranial surface matching the maxilla bone. The geometry of the lattice structure was chosen taking into account the possibility of bone ingrowth into a lattice structure and the manufacturability of the 3D printer. The minimum size of a pore required for a cell to grow into a lattice is at least 0,3 mm.[119] Therefore, a Voronoi-based lattice was built in *Materialise 3-matic 15.0* via `Lattice → Voronoi Based Lattice` with 0,4 mm target pore radius and 0,4 mm thickness and converted to mesh with an organic factor of 1,2. This lattice has a porosity of 57,3%. Lastly, the lattice and the rebuilt model were merged via `Boolean Union`. An isometric, bottom and top view of the redesigned implant can be seen

in figure 3.4, 3.5a and 3.5a. With this redesign, a mass reduction of 13,08% together with an increase of the surface area of 208,71% was achieved.
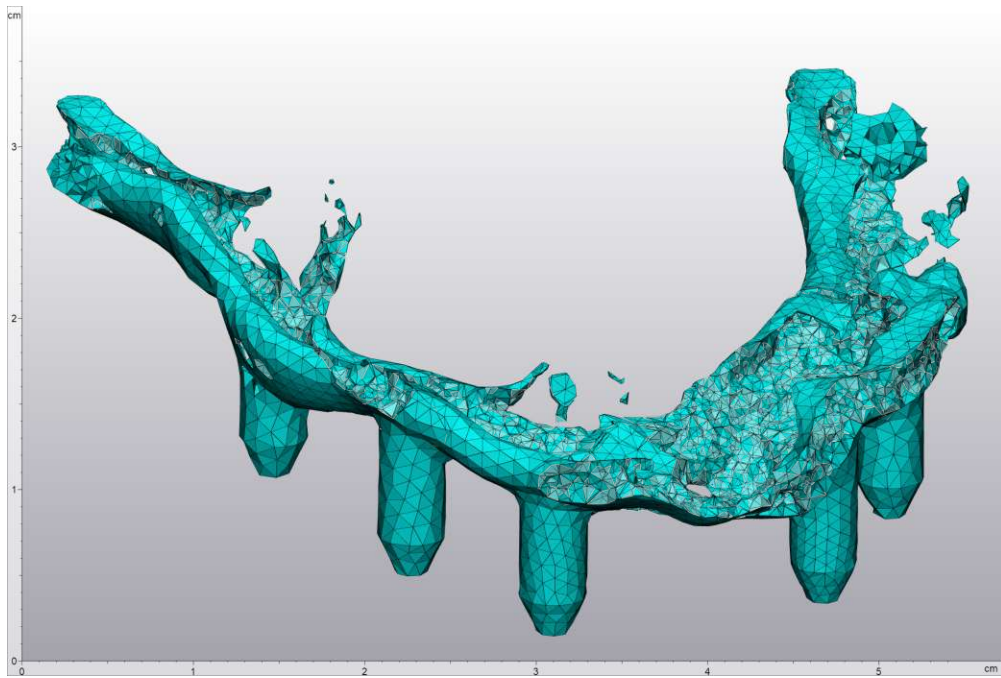
Figure 3.1: Iso plots of the 3 load conditions merged into 1 model in *Autodesk Meshmixer 3.5*.
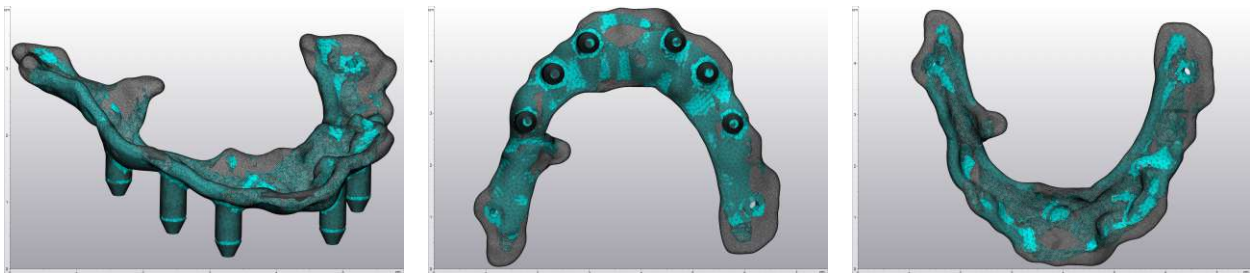
Figure 3.2: Extracted iso surfaces of 3 different load conditions in blue overlaying the transparent initial implant in 3 views. These blue iso surfaces were used as template for the redesign.

Figure 3.3: Rebuilt model according to the iso surface template. Material from the initial model was either added or removed with a continuous 0,5 mm thick outer surface shell in contact with the periosteum.
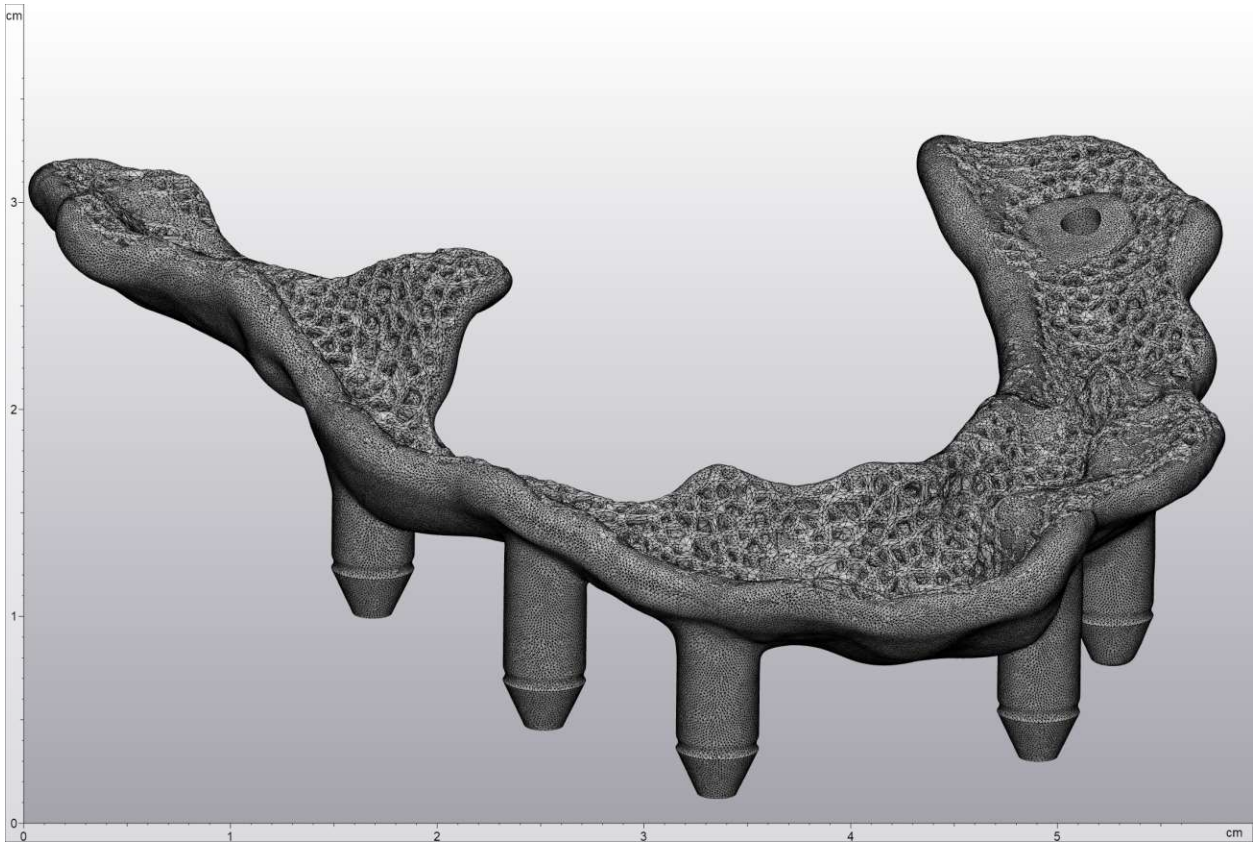
Figure 3.4: Isometric view of the redesign with added lattice structure. Voronoi based lattice with a pore radius and thickness of 0,4 mm.

(a)

(b)
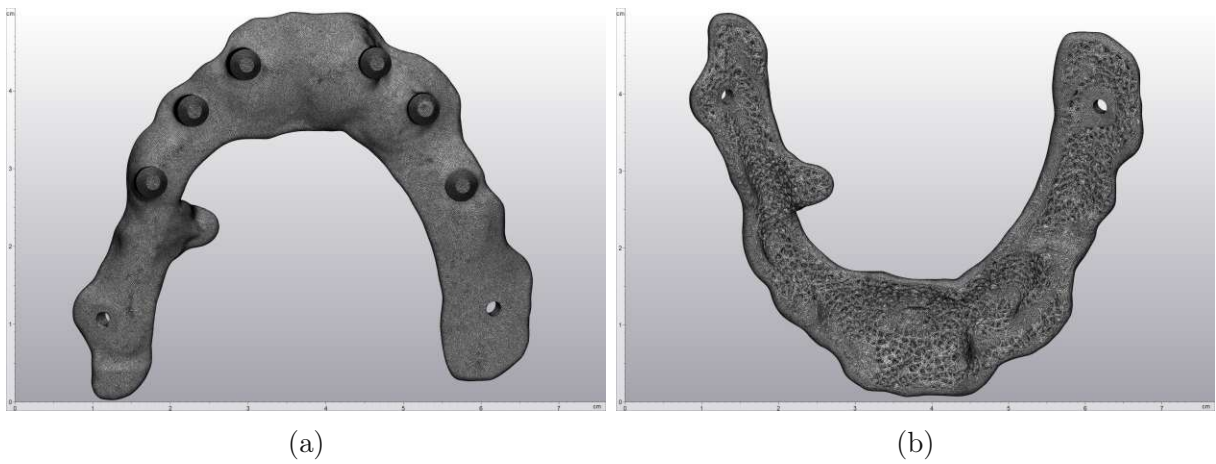
Figure 3.5: (a) Bottom view and (b) top view of the redesigned implant.

3.1 Young's Modulus and Stress Magnification Factor

To test if the redesigned part will withstand the predefined loading conditions, a new simulation model was created. This model was built analogously to the initial model described in chapter 2.2. The lattice structure, however, was shaped as continuous body with a reduced Young's modulus. This Young's modulus was calculated by an in-silico tensile test. Therefore, a cube of 1 cm edge length was built as CAD model. Then, converted into a Voronoi based lattice with 0,4 mm target pore radius and 0,4 mm thickness and converted to a mesh with an organic factor of 1,2 as used in the redesigned implant (Figure 3.6). This lattice cube was then imported into *Altair HyperWorks*. The lattice cube contained of 41130 nodes and 148125 tetrahedrons. Two reference nodes, one on top and one on the bottom of the cube, were established by linking the DOF of all top and all bottom surface nodes respectively. These reference nodes were then constrained in all 6 DOFs and the top reference node was loaded with an `enforced displacement` of 0,1 mm in positive z-direction. The resulting force on the reference node was output and visualized in figure 3.7a. This figure illustrates the lattice cube and a spider web like structure on top, which is the representation of the RBE, connecting all chosen nodes and resulting in a single reference node in the center.

The resulting force in z-direction was 83310 N. This force is needed to derive the effective Young's modulus E_{eff} for the lattice structure. Equation 3.1 gives the mathematical formulation of a linear elastic spring with stiffness c, force F and displacement u.[120] For every elastic system, an equivalent spring stiffness c_{equ} can be computed.[121] A 1D solution can be obtained by equation 3.3. This equivalent spring stiffness can be used to compute E_{eff} of the lattice structure, with A being the area and l the height of the used structure, hence $A = 100$ mm^2 and $l = 10$ mm. Inserting the equivalent spring stiffness c_{equ} from equation 3.3 into equation 3.1 gives equation 3.4 and so the effective Young's modulus. The Young's modulus of a porous material behaves according to a power law formulated in equation 3.6, with E_0 being the Young's modulus of the bulk material, p the porosity, p_{c} the porosity at which the Young's modulus becomes zero and k a parameter describing the morphology of the pores.[122] Since E_{eff} has already been computed and E_0 and p are known, the k $-$ factor of the power law can be computed by choosing $p_{\text{c}} = 1$, hence $k = 1,1278$ for this lattice as equation 3.7 displays. Figure 3.8 shows a graph of the computed power law with obtained k $-$ factor.

$$F = c\, u \tag{3.1}$$

$$F_{\text{z}} = c\, u = 8,331 \cdot 10^4 \text{ N} \tag{3.2}$$

う
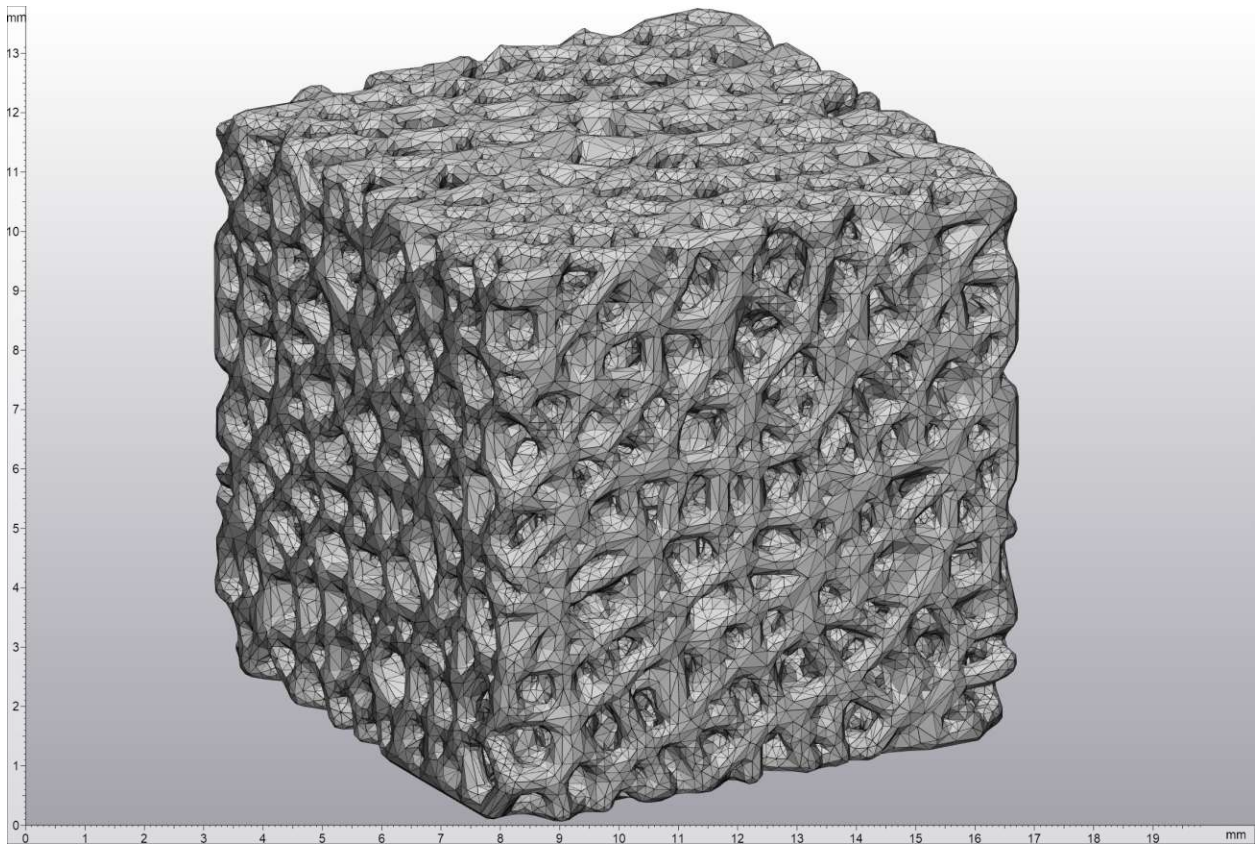
Figure 3.6: Visualization of the lattice cube, displayed in *Materialise 3-matic 15.0*. Voronoi based lattice with a pore radius and thickness of 0,4 mm.
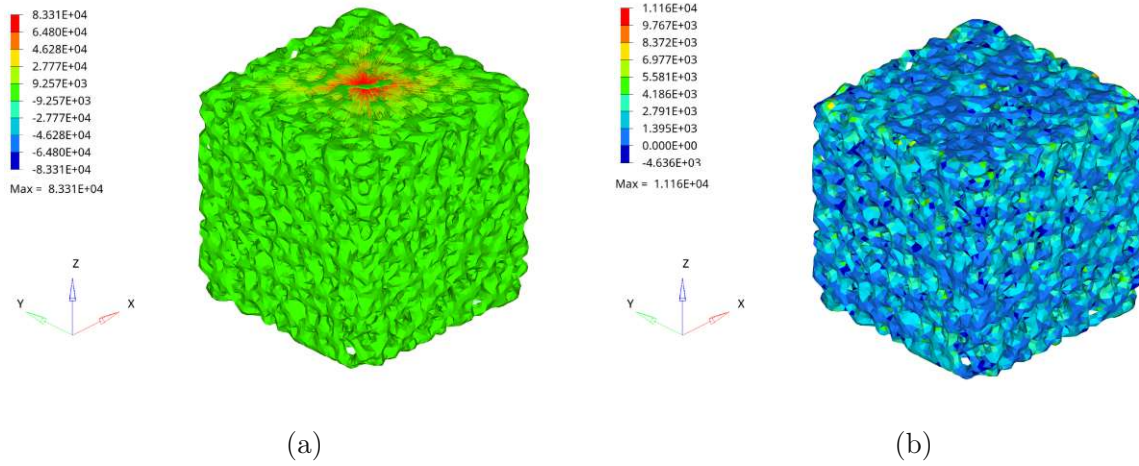
Figure 3.7: Simulation model of the lattice cube. (a) Nodal forces in Z-direction with the maximum force at a reference node at the top (b) absolute maximal principle tensile stress distribution

$$c_{\text{equ}} = \frac{E_{\text{eff}}\, A}{l} \qquad (3.3)$$

$$E_{\text{eff}} = \frac{F_{\text{z}}\, l}{A\, u} = 83,3 \text{ GPa} \qquad (3.4)$$

$$\sigma_{\text{mid}} = \frac{F_{\text{z}}}{A} \qquad (3.5)$$

$$E = E_0 \left(1 - \frac{p}{p_{\text{c}}}\right)^k \qquad (3.6)$$

$$k = \frac{\ln\left(\frac{E_{\text{eff}}}{E_0}\right)}{\ln(1-p)} = \frac{\ln\left(\frac{83,3}{205}\right)}{\ln(1-0,55)} = 1,1278 \qquad (3.7)$$

Because of the complex geometry of a lattice structure, it may have experience a different stress distribution as the equivalent continuous body. The stresses obtained by a simulation of a lattice modeled as continuous body could in reality be higher as derived by this approximation. Therefore, the stresses need to be magnified by a factor. To obtain this factor, the resulting stresses in the simulation of the lattice cube can be compared to an average stress. This average stress σ_{mid} resulting from the force F_{z} was calculated in equation 3.8. The maximum absolute principal stresses of the lattice cube are displayed in figure 3.7b. A ratio
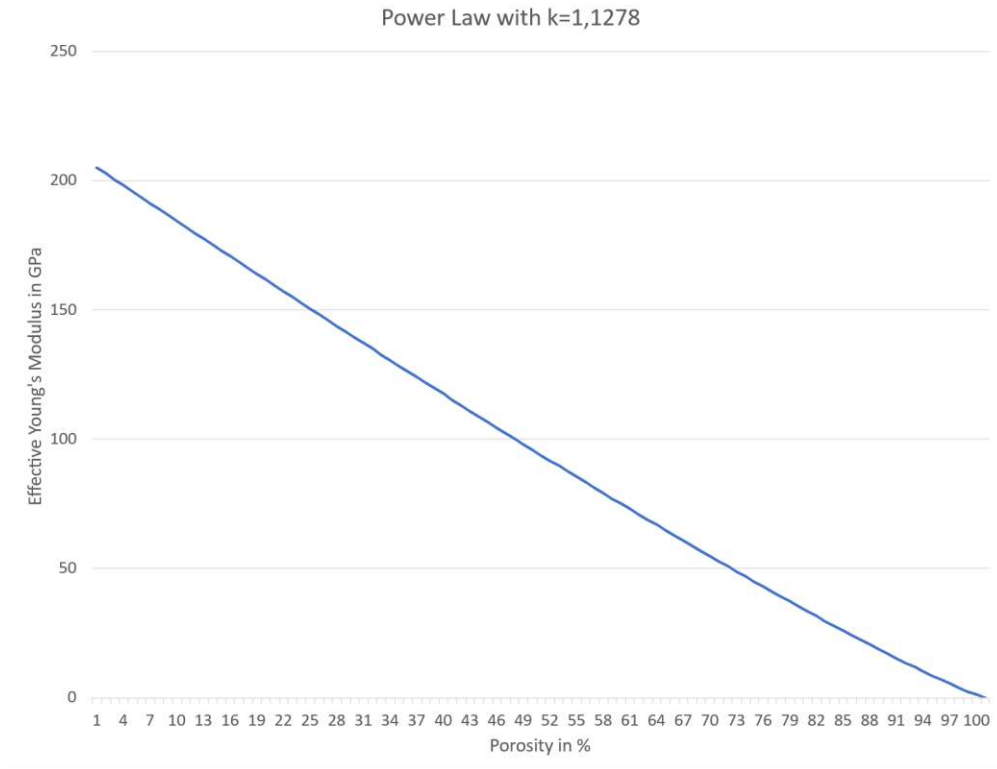
Figure 3.8: Plot of the power law according to equation 3.7 from 0% porosity to 100% porosity.

of $\sigma_{\max}$ to σ_{mid} can be interpreted as stress magnification factor r. This factor implies, that the maximum stress in a lattice structure can be $r-$times higher as displayed by the homogenized model. Consequently, the stress results obtained by the simulation of the redesigned implant must be multiplied for areas in which lattice is present by r. Figures 3.9a and 3.9b show a statistical representation of the absolute maximal principle stresses inside the lattice cube. The presence of a long tail in the distribution and of outliers can be observed. The roughness of the mesh in relation to the cube's size could a possible explanation be, since the cube consists of tetrahedrons of edge length 0,3 mm in a volume of 100mm^3.

So, the maximum occurring stress could have been erroneously selected. With defining the 3 highest stress values as outliers, the maximum stress is turning to $\tilde{\sigma}_{\max} = 8,53 \cdot 10^3$MPa, hence the new stress magnification factor is $r_{\mathrm{new}} = 10,24$, as seen in equation .

$$\sigma_{\mathrm{mid}} = \frac{F_z}{A} = 833 \text{ MPa} \tag{3.8}$$

$$r_{\mathrm{new}} = \frac{\tilde{\sigma}_{\max}}{\sigma_{\mathrm{mid}}} = \frac{8530}{833} = 10,24 \tag{3.9}$$

41
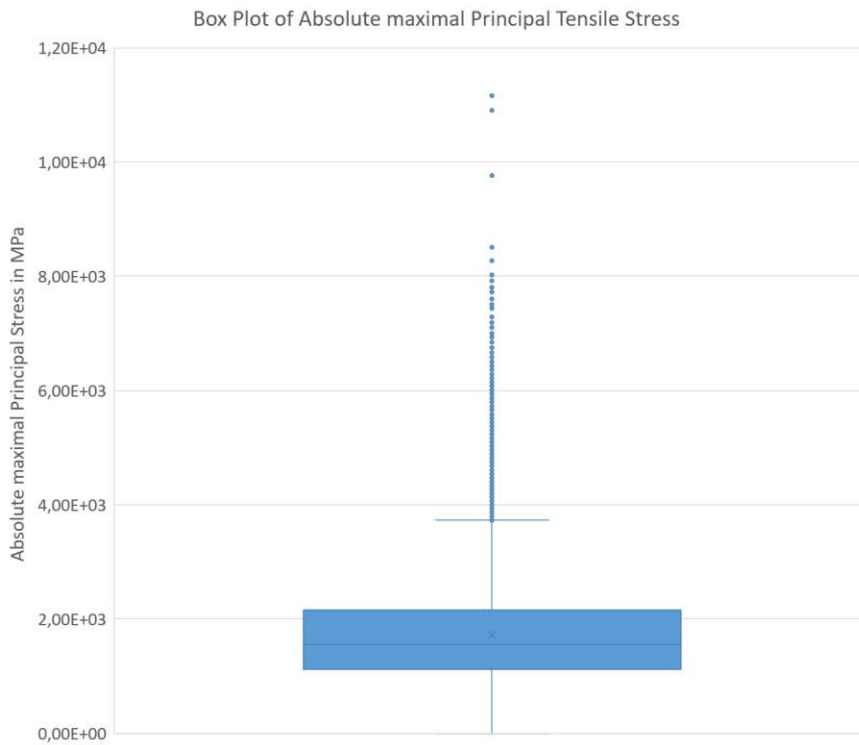
(a)
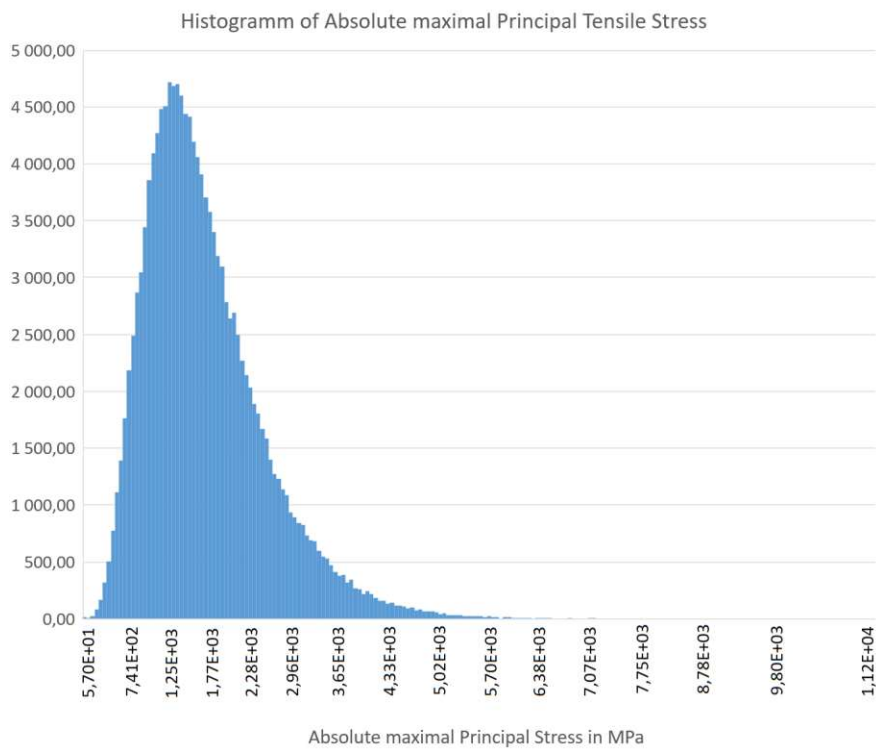
(b)

Figure 3.9: (a) Box plot of the absolute maximal principle stresses obtained from a lattice structure to visualize potential outliers and (b) histogram of the same results

3.2 Model and Stress Evaluation

As mentioned before, the implant was prepared for the simulation analogously to what has been described in chapter 2.2. The preparation, however, was more time-consuming due to the more complex geometry and the many undercuts present, as in the hollow abutments. The redesigned implant without a lattice structure (Figure 3.3) was remeshed with a 1 mm target triangle edge length. The cranial surface was extracted to a new part. Then, the cranial surface of the initial implant, that was already remeshed, was extracted to the new part. These 2 surfaces build up the boundary of the lattice component. By carefully adjusting the mesh of the new part, a closed surface was created. The model of the redesign can be seen in figures 3.10a, 3.10b, 3.11a, 3.11b and 3.12. Finally, a 4 node tetrahedron element volume mesh for all components could be created which lead to mesh properties listed in table 3.1.

Component	Nodes	Elements
Bone	64555	362178
Implant	8277	36314
Implant Lattice	5131	21515
Osseointegration layer	2806	7843
Screw right	172	597
Screw left	112	494

Table 3.1: FE mesh properties used for the second simulation.

The model was again imported into *Altair HyperWorks 2021 Student Edition* as .fem file. Perfect bonding was again achieved between all components leading to 4872 equivalent nodes. The lattice component was assigned with the effective Young's modulus of 83,3 GPa. The loading scenarios and force directions were equivalent to the previously used conditions (Table 2.4).
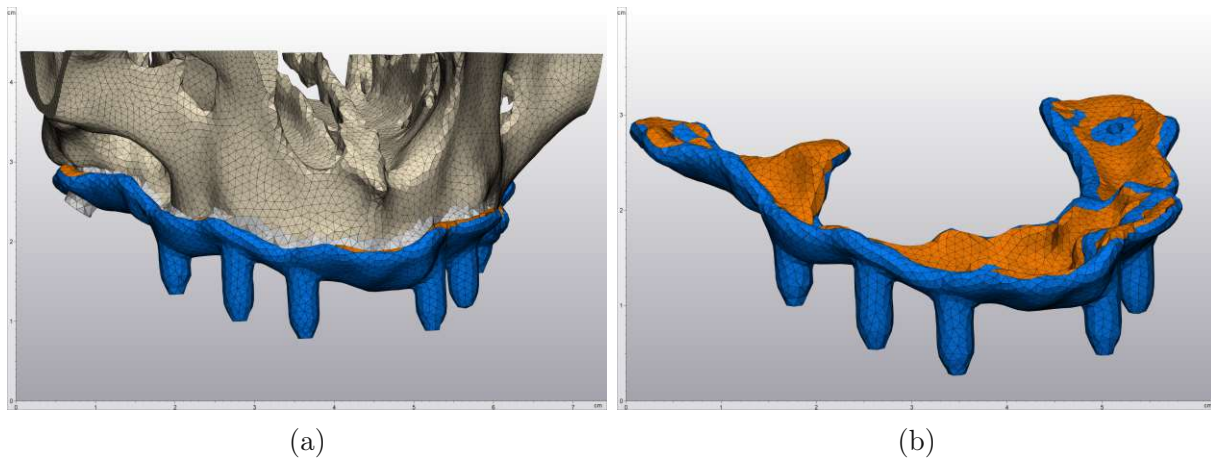
Figure 3.10: (a) Complete simulation model. Blue: implant bulk material; Orange: lattice structure; Grey: the osseointegration layer and the screws; Beige: the bone, and (b) isolated implant model
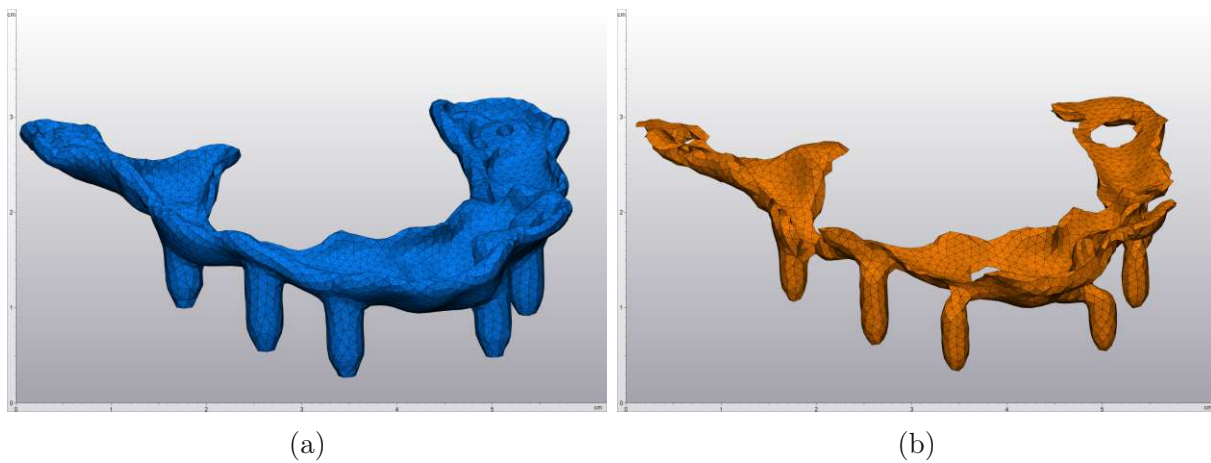
Figure 3.11: (a) Isometric view of the implant model (b) Isometric view of the lattice model as full body of reduced Young's modulus
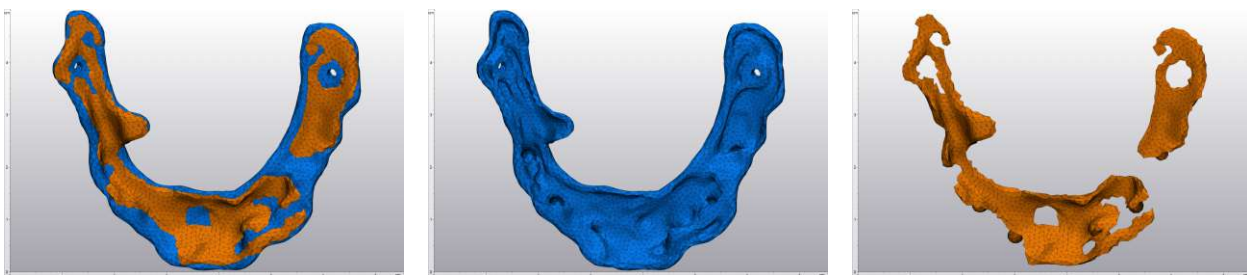
Figure 3.12: Top view of the implant FEA model. Blue: Implant, Orange: Lattice model as full body of reduced Young's modulus.

3.3 Simulation Outcome of the Redesigned Implant

In chapter 2.3.2 the minor differences between the osseointegration layers were apparent, therefore only one scenario with 100% osseointegration was evaluated. In total, 3 different loading cases (Table 3.7a) were simulated and figures 3.13, 3.14a, 3.14b, 3.15a, 3.15b, 3.16a and 3.16b give the results. The absolute maximal principal tensile stresses were considered as the relevant output. The figures also show the implant and the lattice structure independently, to better evaluate the maximal stresses acting on the lattice portion of the implant. As marked in the figures, on the left side loading case molar right, in the middle incisor and on the right side molar left is displayed. The maximum stress in the implant were present in loading case molar right with 61,14 MPa. The maximum stress in the lattice structure occurred likewise in loading case molar right and amounted to 27,21 MPa.
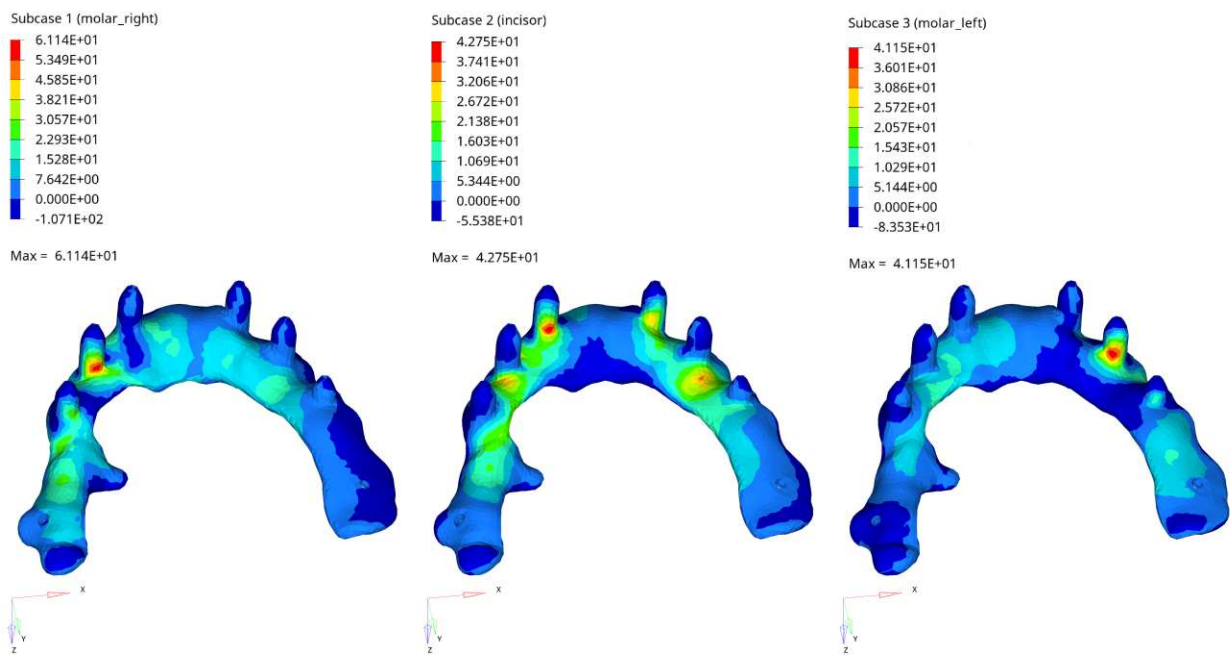
Figure 3.13: Tilted view of the absolute maximum principal stresses of the redesign, colors indicate the calculated element stress in MPa
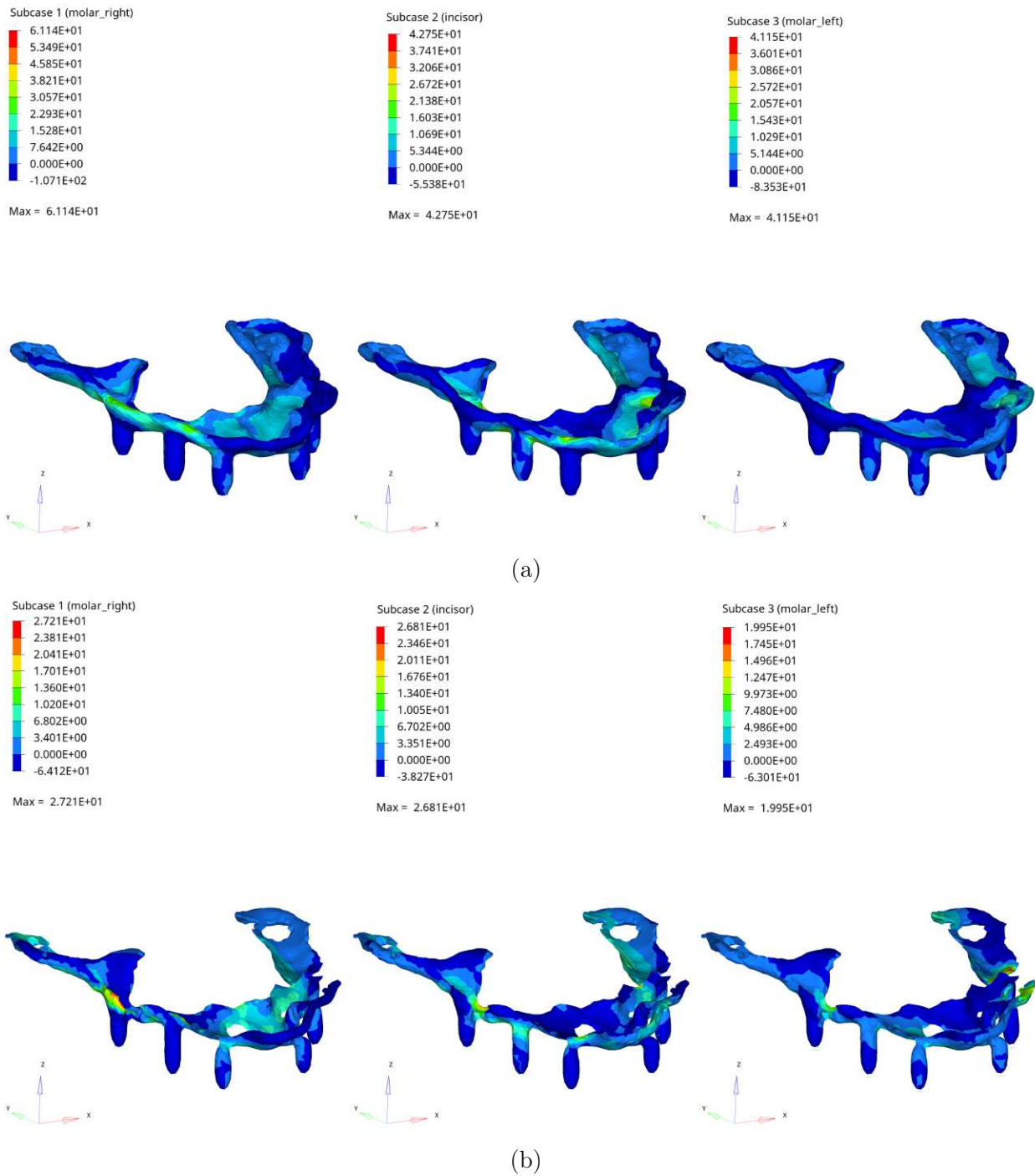
Figure 3.14: Isometric view of the absolute maximal principal stress distribution. (a) the whole implant (b) the lattice structure, colors indicate the calculated element stress in MPa

(a)

(b)
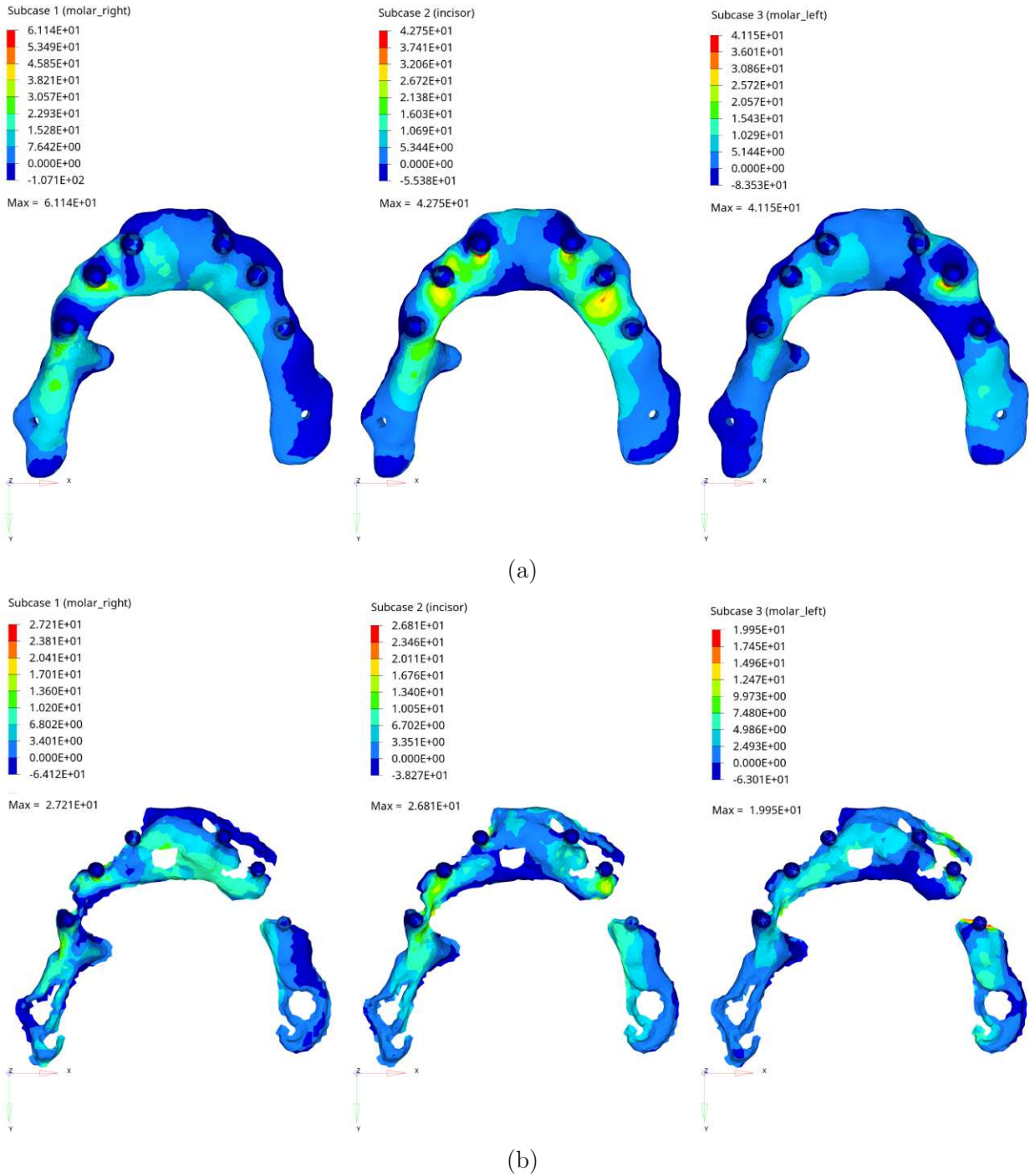
Figure 3.15: Bottom view of the absolute maximal principal stress distribution. (a) the whole implant (b) the lattice structure, colors indicate the calculated element stress in MPa

(a)

(b)
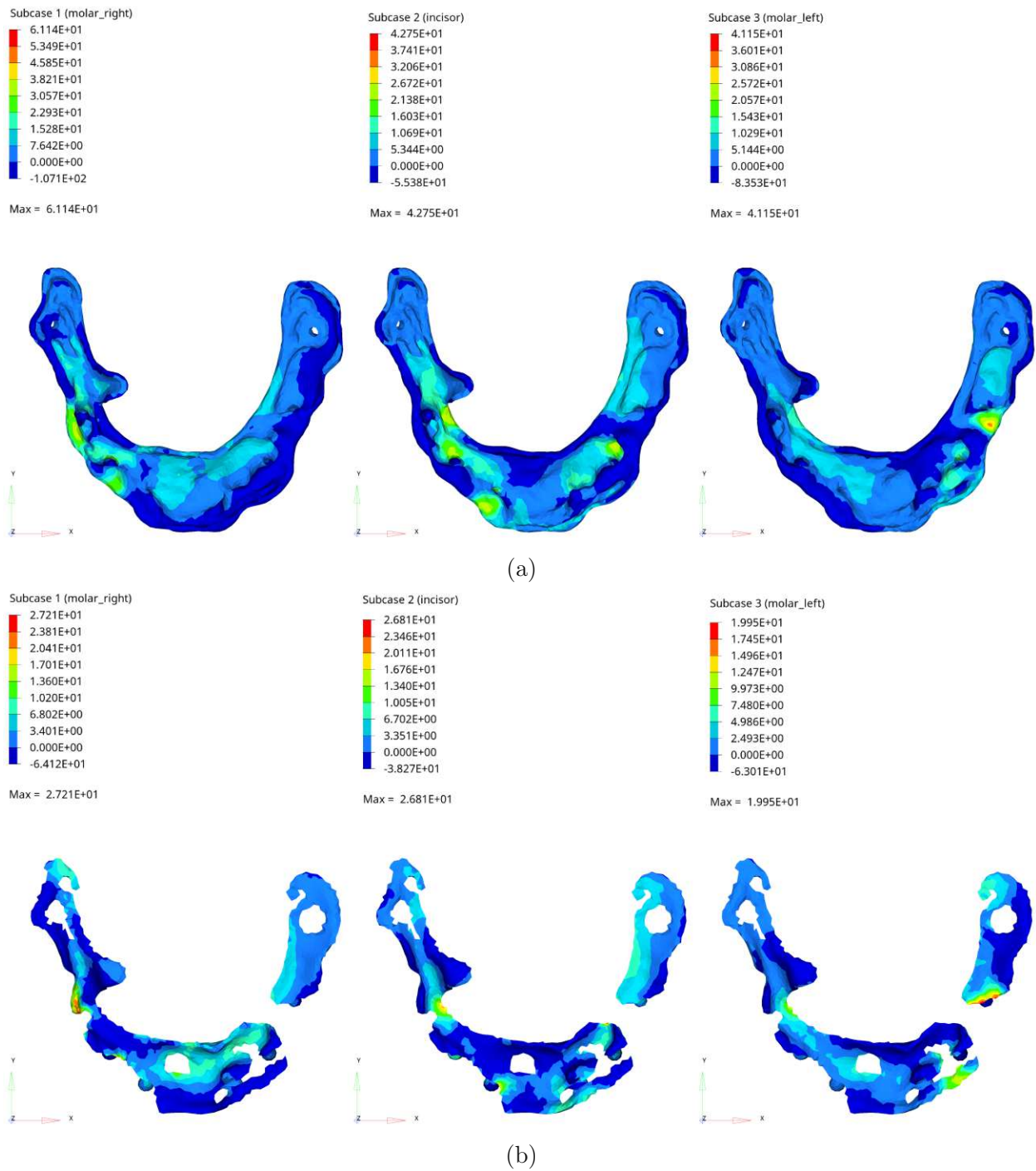
Figure 3.16: Top view of the absolute maximal principal stress distribution. (a) the whole implant (b) the lattice structure, colors indicate the calculated element stress in MPa

3.4 Result Interpretation

Figure 3.13 gives an isometric view of the positive absolute maximum principal stresses of the redesigned part, which are the critical stresses for a ceramic material. 3 red areas are clearly visible which depict a stress concentration at the crossover of the abutment to the implant body. Since the abutments are oriented in order to be aligned with the lips, the occurring mastication forces which are perpendicular to the OP, introduce bending stresses. The maximum occurring stress in the bulk portion of the implant was 61,14 MPa in loading case molar right, hence, well below the ultimate strength of 940 MPa, tolerable by the ceramic material.[98] These areas of stress concentrations, however, could be even optimized by creating a smoother transition from the abutment to the implant body by e.g. increasing the radius.

The inferior view in figure 3.15a and the superior view in 3.16a show no additional stress concentrations.

Figures 3.14b, 3.15b and 3.16b give the corresponding perspective with the isolated lattice structure to evaluate the internal stresses. These must be multiplied by the obtained stress magnification factor $r_{\mathrm{new}} = 10,24$ in response to chapter 3.1.

The maximum principal stress occurring in the lattice is arising in the loading scenario molar right, leading to 27,21 MPa. Multiplying this stress value with r_{new} lead to 278,63 MPa, which is still below the ultimate strength by a factor 3,4, thus suggesting that the lattice would resist this load. Generally, the stresses in the lattice structure are rather small between -64,12 MPa to 27,21 MPa, and they are relatively even in the bone-implant interface. The red areas indicating stress concentration are supposedly resulting from poor contact interactions between the bulk material and the lattice component, so these values can be considered unreliable. Since a conventional bulk subperiosteal implant only rests on the bone, osseointegration won't be encouraged by this surface contact as with an endosseous implants.[123] The almost even stress distribution over the whole implant bone interface together with the osseointegration promoting lattice, however, could lead to major improvements in the treatments outcome.

4 Discussion & Conclusion

This thesis establishes a workflow for an additively manufactured patient-specific subperiosteal implant, where the implant design is guided by FEM and TO. The resulting implant has an optimized lattice structure replacing the bulk material for better bone augmentation and load bearing. The material considered in this approach was yttrium-stabilized zirconium as a potential subperiosteal implant material.

Discussion

This study showed a potential workflow for designing a single piece subperiosteal implant for the maxilla with integrated abutments. Usually, subperiosteal implants are designed in a way, that at least two surgeries, a first operation for the placement of the implant onto the bone, followed by a second operation for placing of the abutments are needed.[4] This research introduces a single surgery design, that increases the patient's convenience while reducing the treatment costs. Additionally, the proposed implant design workflow is based on patient's medical imaging data (CT) ensuring a perfect fit, which is fundamental to eliminate potential osteolysis.[6] Earlier research showed the potential of using AlO_2 ceramic material for a subperiosteal implant design including transmucosal abutments. On the one hand, they did not include a patient specific design and on the other hand did not design the implant as single piece for the whole maxilla.[124] Moreover, this study enlightened the potential of a yttrium-stabilized zirconia for the use in subperiosteal implants. A major advantage of a Yttrium-stabilized Zirconium to an AlO_2 ceramic material is a heavily increased crack resistance, wherefore Yttria-stabilized Zirconia are already adopted in dental, knee, or hip prostheses, however, research which utilize this material for subperiosteal implants was not found.[125] The present study suggest, that the yttrium-stabilized zirconium can withstand the applied loads, thus encouraging further studies, since the feasibility was shown.

With the method of TO, the reduction of weight and material was successfully realized. Furthermore, TO was implemented to obtain comprehensible results for determining locations, which may host a osseointegration promoting lattice structure, which to our knowledge has

not been done before. Therefore, bone augmentation in edentulous patients can be based on a TO-guided design.

The proposed research faces some limitations in terms of design and simulation. The design of the subperiosteal implant for the maxilla was realized according to the pathological maxilla of an edentulous patient. Since the locations of the abutments were already predefined by the physicians, the FEA performed could have given insights in the stress distributions in the bone, and therefore, could suggest a better positioning of the abutments. Additionally, it can be questioned, if 6 abutments are necessary, since on the one hand the occurring stresses in the abutments are easily tolerable in the physiological loading conditions by the material and on the other hand different designs as the "All-on-4" concept, which utilizes 4 abutments, are implemented with other materials such as titanium.[126] Another design aspect can be taken into account, which is a potential bridge between abutments 1.3 and 2.3. This bridge, especially in the case of a patient with a heavily resorbed ridge, could lead to a more favourable stress distribution, due to an extension of the available surface area. In addition, the manufacturing consideration may favor this bridge design, since the post processing step sintering of an implant with such a bridge could lead to less contortions. Both the current design and other design considerations, however, need to be experimentally analyzed.

The optimization starts with the model preparation by meshing the different components which took part in the FEA. A convergence study for the mesh should typically be done, it however was not performed due to licence limitations of the student-edition of the FE-software. Since the aim of this thesis was to test the potential of the method of TO for repeatably and comprehensibly discover locations for lattices, the level of detail applied was therefore sufficient. The obtained output clearly showed understandable and interpretable results, and therefore, an increase of resolution was probably not necessary.

More complex loading scenarios could provide additional insight into the design and optimization. The complexity of the loading cases could be increased by adding potential moment loading to the abutments as well as expanding the simulation with an added dental prosthesis. This could lead to a more realistic simulation model, however, accompanied by a drastic increase of computational complexity. Another way to achieve a more realistic simulation environment could be to differentiate the bone tissue into cancellous and compact bone, also here increasing the complexity of the simulation model. In this thesis, the maxilla was assumed to be of uniform isotropic bone throughout, though in reality bone is anisotropic.[127] This simplification was in correlation with literature.[96]

The method of TO successfully lead to a design of minimal mass, which then was expanded by a lattice. This lattice filled the void to the original implant, since a reduced volume is not desired, given that the implant also serves the purpose of building up the maxillary bone. Which type of lattice and which dimensions the lattice is built of that leads to the best outcome regarding osseointegration has to be studied in further work. The stress anal-

ysis showed potential for the ceramic material, since all occurring stresses are theoretically tolerable. Finally it has to be mentioned, that a computational evaluation alone cannot compensate for physical testing, unless the simulation environment is completely validated.[128] Therefore, it is recommended that the implant be subjected to various physical tests.

Conclusion

This thesis showed the potential to use finite element simulation combined to topological optimization to design and analyze subperiosteal implants made of a yttrium-stabilized zirconium oxide. In particular, topological optimization can be used for systematically and comprehensibly finding potential areas in which lattice structures or even material with different mechanical properties may be included in an implant design. Computational approaches alone cannot be used and experimental data towards the assessment of the overall implant stability and the influence of lattice on osseointegration are sill considered to be necessary to validate the computational findings of this thesis.

List of Figures

List of Tables

Bibliography

[1] S.M. Al-Zubaidi, A.A. Madfa, A.A. Mufadhal, M.A. Aldawla, O.S. Hameed, and X.G. Yue. Improvements in clinical durability from functional biomimetic metallic dental implants. *Frontiers in Materials*, 7, 2020. doi: 10.3389/fmats.2020.00106.

[2] Global Burden of Disease Collaborative Network. Global Burden of Disease Study 2019 (GBD 2019). Seattle: Institute of Health Metrics and Evaluation (IHME); 2020. Available from http://ghdx.healthdata.org/gbd-results-tool.

[3] G.G. Nascimento, F.R.M. Leite, D.A. Conceição, C.P. Ferrúa, A. Singh, and F.F. Demarco. Is there a relationship between obesity and tooth loss and edentulism? A systematic review and meta-analysis: Obesity and tooth loss. *Obesity Reviews*, 17(7): 587–598, July 2016. doi: 10.1111/obr.12418.

[4] C.E. Misch. *Dental Implant Prosthetics*. Elservier Mosby, 1. edition, 2004. ISBN 978-0-323-07896-2.

[5] S. Bauer and D. Paulus. Computational Simulation as an Innovative Approach in Personalized Medicine. In *Innovations in Spinal Deformities and Postural Disorders*. InTech, September 2017. ISBN 978-953-51-3542-5. doi: 10.5772/intechopen.68835.

[6] T.M. Nguyen, J.-B. Caruhel, and R.H. Khonsari. A subperiosteal maxillary implant causing severe osteolysis. *Journal of Stomatology, Oral and Maxillofacial Surgery*, 119 (6):523–525, December 2018. doi: 10.1016/j.jormas.2018.06.007.

[7] M.Y. Mommaerts. Evolutionary steps in the design and biofunctionalization of the additively manufactured sub-periosteal jaw implant 'AMSJI' for the maxilla. *International Journal of Oral and Maxillofacial Surgery*, 48(1):108–114, January 2019. doi: 10.1016/j.ijom.2018.08.001.

[8] H.M. Frost. From Wolff's law to the Utah paradigm: Insights about bone physiology and its clinical applications. *The Anatomical Record*, 262(4):398–419, April 2001. doi: 10.1002/ar.1049.

[9] A. Roth. Periprothetische osteopenie. *Osteologie*, 24:158–162, 01 2015. doi: 10.1055/s-0037-1622063.

[10] B. Klein. *FEM*. Springer Fachmedien Wiesbaden, Wiesbaden, 2015. ISBN 978-3-658-06053-4. doi: 10.1007/978-3-658-06054-1.

[11] Z. Yang. *Finite Element Analysis for Biomedical Engineering Applications*. CRC Press, 1 edition, March 2019. ISBN 978-0-429-06126-4. doi: 10.1201/9780429061264.

[12] M.I.Z. Ridzwan, S. Shuib, A.Y. Hassan, A.A. Shokri, and M.N.M. Ibrahim. Optimization in implant topology to reduce stress shielding problem. 6(13):2768–2773. doi: 10.3923/jas.2006.2768.2773.

[13] J. Fang, G. Sun, N. Qiu, N.H. Kim, and Q. Li. On design optimization for structural crashworthiness and its state of the art. 55(3):1091–1119, mar 2017. doi: 10.1007/s00158-016-1579-y.

[14] G.I.N. Rozvany and T. Lewiński. *Topology Optimization in Structural and Continuum Mechanics*, volume CISM International Centre for Mechanical Sciences. Springer Wien Heidelberg New York Dordrecht London, Udine, 2014. ISBN 978-3-7091-1642-5. doi: 10.1007/978-3-7091-1643-2.

[15] N. Wu, S. Li, B. Zhang, C. Wang, B. Chen, Q. Han, and J. Wang. The advances of topology optimization techniques in orthopedic implants: A review. *Medical & Biological Engineering & Computing*, 59(9):1673–1689, 2021. doi: 10.1007/s11517-021-02361-7.

[16] A. Carnicero, A. Peláez, A. Restoy-Lozano, I. Jacquott, and R. Perera. Improvement of an additively manufactured subperiosteal implant structure design by finite elements based topological optimization. *Scientific Reports*, 11(1):15390, December 2021. doi: 10.1038/s41598-021-94980-1.

[17] V. Dhinakarsamy and R. Jayesh. Osseointegration. *Journal of Pharmacy and Bioallied Sciences*, 7(5):228, 2015. doi: 10.4103/0975-7406.155917.

[18] R.R. Resnik. *Misch's contemporary implant dentistry*. Elsevier, St. Louis, 4. edition, 2020. ISBN 978-0-323-39155-9.

[19] D.P. Papazoglou. *Additively Manufactured Lattices for Orthopedic Implants and Process Monitoring of Laser-Powder Bed Fusion using Neural Networks*. PhD thesis, The School of Engineering of the University of Dayton, May 2019.

[20] D.F. Ângelo and J.R. Vieira Ferreira. The role of custom-made subperiosteal implants for rehabilitation of atrophic jaws - A case report. *Annals of Maxillofacial Surgery*, 10 (2):507, 2020. doi: 10.4103/ams.ams_263_20.

[21] C. Mangano, A. Bianchi, F.G. Mangano, J. Dana, M. Colombo, I. Solop, and O. Admakin. Custom-made 3D printed subperiosteal titanium implants for the prosthetic restoration of the atrophic posterior mandible of elderly patients: a case series. *3D Printing in Medicine*, 6(1):1, December 2020. doi: 10.1186/s41205-019-0055-x.

[22] L.P. Webber, H.L. Chan, and H.L. Wang. Will Zirconia Implants Replace Titanium Implants? *Applied Sciences*, 11(15):6776, July 2021. doi: 10.3390/app11156776.

[23] D. Vogel, D. Kluess, P. Bergschmidt, W. Mittelmeier, and R. Bader. Ceramics for joint replacement. In *Joint Replacement Technology*, pages 123–143. Elsevier, 2021. ISBN 978-0-12-821082-6. doi: 10.1016/B978-0-12-821082-6.00012-1.

[24] E. Emami, R.F. De Souza, M. Kabawat, and J.S. Feine. The Impact of Edentulism on Oral and General Health. *International Journal of Dentistry*, 2013:1–7, 2013. doi: 10.1155/2013/498305.

[25] D. Kandelman, S. Arpin, R.J. Baez, P.C. Baehni, and P.E. Petersen. Oral health care systems in developing and developed countries: Oral health care systems. *Periodontology 2000*, 60(1):98–109, October 2012. doi: 10.1111/j.1600-0757.2011.00427.x.

[26] I. Polzer. Edentulism as part of the general health problems of elderly adults*. *International Dental Journal*, 60:13, 2010. doi: 10.1922/IDJ_2184Polzer13.

[27] Z. Jakab. Inequalities in health: challenges and opportunities in Europe. *21st Congress of the European Association of Dental Public Health*, October 2016. URL https://www.euro.who.int/__data/assets/pdf_file/0015/320064/RD-presentation-Inequalities-in-health-1-October-2016,-Budapest.pdf.

[28] S.O. Griffin, P.M. Griffin, C.H. Li, W.D. Bailey, D. Brunson, and J.A. Jones. Changes in Older Adults' Oral Health and Disparities: 1999 to 2004 and 2011 to 2016. *Journal of the American Geriatrics Society*, 67(6):1152–1157, June 2019. doi: 10.1111/jgs.15777.

[29] Oral Health Surveillance Report: Trends in Dental Caries and Sealants, Tooth Retention, and Edentulism, United States 1999-2004 to 2011-2016. Technical report, Center for Disease Control and Prevention, US Dept of Health and Human Services, Atlanta, GA, 2019.

[30] H. Tilg and A.R. Moschen. Adipocytokines: mediators linking adipose tissue, inflammation and immunity. *Nature Reviews Immunology*, 6(10):772–783, October 2006. doi: 10.1038/nri1937.

[31] P.J. Slootweg, editor. *Dental and Oral Pathology*. Encyclopedia of Pathology. Springer International Publishing, 2016. ISBN 978-3-319-28084-4. doi: 10.1007/978-3-319-28085-1.

[32] I.L.C. Chapple, F. Van der Weijden, C. Doerfer, D. Herrera, L. Shapira, D. Polak, P. Madianos, A. Louropoulou, E. Machtei, N. Donos, H. Greenwell, A.J. Van Winkelhoff, B. Eren Kuru, N. Arweiler, W. Teughels, M. Aimetti, A. Molina, E. Montero, and F. Graziani. Primary prevention of periodontitis: managing gingivitis. *Journal of Clinical Periodontology*, 42:S71–S76, April 2015. doi: 10.1111/jcpe.12366.

[33] R. Zelig, R. Touger-Decker, M. Chung, and L. Byham-Gray. Associations Between Tooth Loss, With or Without Dental Prostheses, and Malnutrition Risk in Older Adults: A Systematic Review. *Topics in Clinical Nutrition*, 31(3):232–247, July 2016. doi: 10.1097/TIN.0000000000000077.

[34] M.G. Cademartori, M.T. Gastal, G.G. Nascimento, F.F.o Demarco, and M.B. Corrêa. Is depression associated with oral health outcomes in adults and elders? A systematic review and meta-analysis. *Clinical Oral Investigations*, 22(8):2685–2702, November 2018. doi: 10.1007/s00784-018-2611-y.

[35] E. Mijiritsky, Y. Lerman, O. Mijiritsky, A. Shely, J. Meyerson, and M. Shacham. Development and Validation of a Questionnaire Evaluating the Impact of Prosthetic Dental Treatments on Patients' Oral Health Quality of Life: A Prospective Pilot Study. *International Journal of Environmental Research and Public Health*, 17(14):5037, July 2020. doi: 10.3390/ijerph17145037.

[36] Y. Matsuyama, H. Jürges, and S. Listl. The Causal Effect of Education on Tooth Loss: Evidence From United Kingdom Schooling Reforms. *American Journal of Epidemiology*, 188(1):87–95, January 2019. doi: 10.1093/aje/kwy205.

[37] A.R. Ahmadinia, D. Rahebi, M. Mohammadi, M. Ghelichi-Ghojogh, A. Jafari, F. Esmaielzadeh, and A. Rajabi. Association between type 2 diabetes (T2D) and tooth loss: a systematic review and meta-analysis. *BMC Endocrine Disorders*, 22(1):100, December 2022. doi: 10.1186/s12902-022-01012-8.

[38] R.J. Genco and W.S. Borgnakke. Diabetes as a potential risk for periodontitis: association studies. *Periodontology 2000*, 83(1):40–45, June 2020. doi: 10.1111/prd.12270.

[39] R. Brandes, F. Lang, and R.F. Schmidt, editors. *Physiologie des Menschen: mit Pathophysiologie*. Springer-Lehrbuch. Springer Berlin Heidelberg, Berlin, Heidelberg, 2019. ISBN 978-3-662-56467-7. doi: 10.1007/978-3-662-56468-4.

[40] S. Coleman and R. Grover. The anatomy of the aging face: Volume loss and changes in 3-dimensional topography. *Aesthetic Surgery Journal*, 26(1):S4–S9, January 2006. doi: 10.1016/j.asj.2005.09.012.

[41] M.A. Peres, G. Tsakos, P.R. Barbato, D.A.S. Silva, and K.G. Peres. Tooth loss is associated with increased blood pressure in adults - a multidisciplinary population-based study. *Journal of Clinical Periodontology*, 39(9):824–833, September 2012. doi: 10.1111/j.1600-051X.2012.01916.x.

[42] R.G. Watt, G. Tsakos, C. de Oliveira, and M. Hamer. Tooth Loss and Cardiovascular Disease Mortality Risk – Results from the Scottish Health Survey. *PLoS ONE*, 7(2): e30797, February 2012. doi: 10.1371/journal.pone.0030797.

[43] F. Teng, F.Y. Du, H.Z. Chen, R.P. Jiang, and T.M. Xu. Three-dimensional analysis of the physiologic drift of adjacent teeth following maxillary first premolar extractions. *Scientific Reports*, 9(1):14549, December 2019. doi: 10.1038/s41598-019-51057-4.

[44] F.A. Al-Quran, R.F. Al-Ghalayini, and B.N. Al-Zu'bi. Single-tooth replacement: factors affecting different prosthetic treatment modalities. *BMC Oral Health*, 11(1):34, December 2011. doi: 10.1186/1472-6831-11-34.

[45] R. Smeets, L. Matthies, P. Windisch, M. Gosau, R. Jung, N. Brodala, M. Stefanini, J. Kleinheinz, M. Payer, A. Henningsen, B. Al-Nawas, and C. Knipfer. Horizontal

augmentation techniques in the mandible: a systematic review. *International Journal of Implant Dentistry*, 8(1):23, December 2022. doi: 10.1186/s40729-022-00421-7.

[46] A. Matsumura, T. Nakano, S. Ono, A. Kaminaka, H. Yatani, and D. Kabata. Multivariate analysis of causal factors influencing accuracy of guided implant surgery for partial edentulism: a retrospective clinical study. *International Journal of Implant Dentistry*, 7(1):28, December 2021. doi: 10.1186/s40729-021-00313-2.

[47] J.I. Cawood and R.A. Howell. A classification of the edentulous jaws. *International Journal of Oral and Maxillofacial Surgery*, 17(4):232–236, August 1988. doi: 10.1016/S0901-5027(88)80047-X.

[48] E. Demirdjan. The Complete Maxillary Subperiosteal Implant: An Overview of its Evolution. *Journal of Oral Implantology*, 24(4):196–197, October 1998. doi: 10.1563/1548-1336(1998)24<196:TCMSIA>2.0.CO;2.

[49] M. Uezono, K. Takakuda, M. Kikuchi, S. Suzuki, and K. Moriyama. Hydroxyapatite/-collagen nanocomposite-coated titanium rod for achieving rapid osseointegration onto bone surface: HAp/Col Coating for Rapid Osseointegration onto Bone Surface. *Journal of Biomedical Materials Research Part B: Applied Biomaterials*, 101B(6):1031–1038, August 2013. doi: 10.1002/jbm.b.32913.

[50] C. Van den Borre, M. Rinaldi, B. De Neef, N.A.J. Loomans, E. Nout, L. Van Doorne, I. Naert, C. Politis, H. Schouten, G. Klomp, L. Beckers, M.M. Freilich, and M.Y. Mommaerts. Radiographic Evaluation of Bone Remodeling after Additively Manufactured Subperiosteal Jaw Implantation (AMSJI) in the Maxilla: A One-Year Follow-Up Study. *Journal of Clinical Medicine*, 10(16):3542, August 2021. doi: 10.3390/jcm10163542.

[51] M. Schünke, E. Schulte, U. Schumacher, M. Voll, K.H. Wesker, and C. Stefan, editors. *Thieme Atlas of Anatomy*. Thieme Medical Publishers, Inc., 3rd edition edition. ISBN 978-1-68420-086-3.

[52] A. Waldeyer and J. Fanghänel, editors. *Anatomie des Menschen*. de Gruyter, Berlin, 17. edition, 2003. ISBN 978-3-11-016561-6.

[53] J. Patel, R.Y. Jablonski, and L.A. Morrow. Complete dentures: an update on clinical assessment and management: part 1. 225(8):707–714. doi: 10.1038/sj.bdj.2018.866.

[54] G. Zarb, J.A. Hobkirk, S.E. Eckert, and R.F. Jacob. *Prosthodontic Treatment for Edentulous Patients*. Mosby, 13. edition. ISBN 978-0-323-07844-3.

[55] F. Boschetti, G. Pennati, F. Gervaso, G.M. Peretti, and G. Dubini. Biomechanical properties of human articular cartilage under compressive loads. 41(3):159–166. PMID:15299249.

[56] E.F. Morgan, G.U. Unnikrisnan, and A.I. Hussein. Bone mechanical properties in healthy and diseased states. 20(1):119–143. doi: 10.1146/annurev-bioeng-062117-121139.

[57] M. Pawlaczyk, M. Lelonkiewicz, and M. Wieczorowski. Age-dependent biomechanical properties of the skin. 5:302–306. doi: 10.5114/pdia.2013.38359.

[58] S.L. Sing, J. An, W.Y. Yeong, and F.E. Wiria. Laser and electron-beam powder-bed additive manufacturing of metallic implants: A review on processes, materials and designs. October 2015. doi: 10.1002/jor.23075.

[59] W. Jamróz, J. Szafraniec, M. Kurek, and R. Jachowicz. 3D Printing in Pharmaceutical and Medical Applications – Recent Achievements and Challenges. 35(9):176, September 2018. doi: 10.1007/s11095-018-2454-x.

[60] M.P. Chae, W.M. Rozen, P.G. McMenamin, M.W. Findlay, R.T. Spychal, and D.J. Hunter-Smith. Emerging Applications of Bedside 3D Printing in Plastic Surgery. 2. doi: 10.3389/fsurg.2015.00025.

[61] S.P. Krishnan, A. Dawood, R. Richards, J. Henckel, and A.J. Hart. A review of rapid prototyped surgical guides for patient-specific total knee replacement. 94-B(11):1457–1461. doi: 10.1302/0301-620X.94B11.29350.

[62] R. Kramme, editor. *Medizintechnik: Verfahren - Systeme - Informationsverarbeitung*. Springer, 4. edition. ISBN 978-3-642-16186-5.

[63] N. Tan and R. van Arkel. Topology optimisation for compliant hip implant design and reduced strain shielding. 14(23):7184, November 2021. doi: 10.3390/ma14237184.

[64] J. Tesk and G. Widera. Stress Distribution in Bone Arising from Loading on Endosteal Dental Implants. *Journal of biomedical materials research*, 7:251–61, 05 1973. doi: 10.1002/jbm.820070317.

[65] C.L. Chang, C.S. Chen, C.H. Huang, and M.L. Hsu. Finite element analysis of the dental implant using a topology optimization method. 34(7):999–1008. doi: 10.1016/j.medengphy.2012.06.004.

[66] K. Knothe and H. Wessels. *Finite Elemente.* Springer Berlin Heidelberg, Berlin, Heidelberg, 2017. ISBN 978-3-662-49351-9. doi: 10.1007/978-3-662-49352-6.

[67] F. Hartmann and C. Katz. *Structural analysis with finite elements.* Springer, Berlin, New York, 2. edition, 2007. ISBN 978-3-540-49698-4.

[68] T. Schmidt. *Potentialbewertung generativer Fertigungsverfahren für Leichtbauteile.* Springer, Berlin, Heidelberg, 2016. ISBN 978-3-662-52995-9. doi: 10.1007/978-3-662-52996-6.

[69] V. Kandemir, O. Dogan, and U. Yaman. Topology optimization of 2.5d parts using the SIMP method with a variable thickness approach. 17:29–36, 2018. doi: 10.1016/j.promfg.2018.10.009.

[70] C.H. Li, C.H. Wu, and C.L. Lin. Design of a patient-specific mandible reconstruction implant with dental prosthesis for metal 3d printing using integrated weighted topology optimization and finite element analysis. 105:103700, May 2020. doi: 10.1016/j.jmbbm.2020.103700.

[71] A. Arra and P. Dhatrak. A review on techniques employed for topology optimization in implant dentistry. *AIP Conference Proceedings*, page 100009, July 2021. doi: 10.1063/5.0057920.

[72] A. Kamrani and E.A. Nasr. *Rapid Prototyping: Theory and Practice.* Manufacturing Systems Engineering Series. Springer, 2006. ISBN 978-0-387-23290-4.

[73] I. Gibson, D. Rosen, B. Stucker, and M. Khorasani. *Additive Manufacturing Technologies.* Springer International Publishing, Cham, 2021. ISBN 978-3-030-56126-0. doi: 10.1007/978-3-030-56127-7.

[74] S. Shakibania, M. Khakbiz, C.K. Bektas, L. Ghazanfari, M.T. Banizi, and K.B. Lee. A review of 3D printing technology for rapid medical diagnostic tools. 7(4):315–324, 2022. doi: 10.1039/D1ME00178G.

[75] M.A. Khan and J.T. Winowlin Jappes, editors. *Innovations in Additive Manufacturing.* Springer Tracts in Additive Manufacturing. Springer International Publishing, Cham, 2022. ISBN 978-3-030-89400-9. doi: 10.1007/978-3-030-89401-6.

[76] M. Javaid and A. Haleem. Current status and applications of additive manufacturing in dentistry: A literature-based review. *Journal of Oral Biology and Craniofacial Research*, 9(3):179–185, July 2019. doi: 10.1016/j.jobcr.2019.04.004.

[77] G2 PRINTER Genera Printer GmbH. https://genera3d.com/system-products/. Accessed: July, 2022.

[78] J. Stampfl. 308.106 Biocompatible Materials Course handout, Winter semester 2020/21. TU Wien.

[79] H. Salmang and H. Scholze, editors. *Keramik.* Springer, 7. edition, 2007. ISBN 978-3-540-63273-3.

[80] M.F. Kunrath, S. Gupta, F. Lorusso, A. Scarano, and S. Noumbissi. Oral Tissue Interactions and Cellular Response to Zirconia Implant-Prosthetic Components: A Critical Review. 14(11):2825. doi: 10.3390/ma14112825.

[81] M. Schwentenwein and J. Homa. Additive Manufacturing of Dense Alumina Ceramics. 12(1):1–7. doi: 10.1111/ijac.12319.

[82] H. Nakai, M. Inokoshi, K. Nozaki, K. Komatsu, S. Kamijo, H. Liu, M. Shimizubata, S. Minakuchi, B. Van Meerbeek, J. Vleugels, and F. Zhang. Additively Manufactured Zirconia for Dental Applications. 14(13):3694. doi: 10.3390/ma14133694.

[83] R. Danzer, T. Lube, P. Supancic, and R. Damani. Fracture of Ceramics. *Advanced Engineering Materials*, 10(4):275–298, April 2008. doi: 10.1002/adem.200700347.

[84] K. Willemsen, R. Nizak, H.J. Noordmans, R.M. Castelein, H. Weinans, and M.C. Kruyt. Challenges in the design and regulatory approval of 3d-printed surgical implants: a two-case series. 1(4):e163–e171, August 2019. doi: 10.1016/S2589-7500(19) 30067-6.

[85] The Glossary of Prosthodontic Terms. 117(5):C1–e105, May 2017. doi: 10.1016/j. prosdent.2016.12.001.

[86] M. Esposito, J.M. Hirsch, U. Lekholm, and P. Thomsen. Biological factors contributing to failures of osseointegrated oral implants, (II). etiopathogenesis: Biological factors contributing to failures of osseointegrated oral implants, (II). etiopathogenesis. 106(3): 721–764. doi: 10.1046/j.0909-8836..t01-6-.x.

[87] E. De Moor, S.E.F. Huys, G.H. van Lenthe, M.Y. Mommaerts, and J. Vander Sloten. Mechanical evaluation of a patient-specific additively manufactured subperiosteal jaw implant (AMSJI) using finite-element analysis. *International Journal of Oral and Maxillofacial Surgery*, May 2021. doi: 10.1016/j.ijom.2021.05.011.

[88] C. Drago and K. Howell. Concepts for designing and fabricating metal implant frameworks for hybrid implant prostheses: Metal implant frameworks for hybrid prostheses. 21(5):413–424, July 2012. doi: 10.1111/j.1532-849X.2012.00835.x.

[89] M. Sato, M. Motoyoshi, M. Hirabayashi, K. Hosoi, N. Mitsui, and N. Shimizu. Inclination of the occlusal plane is associated with the direction of the masticatory movement path. 29(1):21–25, 2007. doi: 10.1093/ejo/cjl036.

[90] G.S. Trento, F.B.R. Bernabé, D.J. Costa, N.L.B. Rebellato, L.E. Klüppel, and R. Scariot. Clinical and radiographic evaluation of maxillary central incisors exposure in patients undergoing maxillary advancement. 20(6):52–59, December 2015. doi: 10.1590/2177-6709.20.6.052-059.oar.

[91] G. Isgró, O. Addison, and G.J.P. Fleming. Transient and residual stresses induced during the sintering of two dentin ceramics. 27(4):379–385, April 2011. doi: 10.1016/j.dental.2010.11.018.

[92] N.H. Kim. *Introduction to Nonlinear Finite Element Analysis*. Springer US, 2015. ISBN 978-1-4419-1745-4. doi: 10.1007/978-1-4419-1746-1.

[93] *HyperMesh Introduction Pre-Processing for Finite Element Analysis*. Altair engineering, Inc., 2014.

[94] S.Y. Ertem, S. Uckan, and U.A. Ozden. The comparison of angular and curvilinear marginal mandibulectomy on force distribution with three dimensional finite element analysis. 41(3):e54–e58, April 2013. doi: 10.1016/j.jcms.2012.07.014.

[95] A.M.A. Mohamed, M.G. Askar, and M.M.B. El Homossany. Stresses induced by one piece and two piece dental implants in all-on-4® implant supported prosthesis under

simulated lateral occlusal loading: non linear finite element analysis study. 22(1):196, 2022. doi: 10.1186/s12903-022-02228-9.

[96] S. Prasadh, S. Suresh, K.L. Hong, A. Bhargav, V. Rosa, and R.C.W. Wong. Biomechanics of alloplastic mandible reconstruction using biomaterials: The effect of implant design on stress concentration influences choice of material. *Journal of the Mechanical Behavior of Biomedical Materials*, 103:103548, March 2020. doi: 10.1016/j.jmbbm.2019.103548.

[97] D.M. Robertson and D.C. Smith. Compressive strength of mandibular bone as a function of microstructure and strain rate. *Journal of Biomechanics*, 11(10):455–471, 1978. doi: https://doi.org/10.1016/0021-9290(78)90057-X.

[98] Lithoz GmbH. Lithoz Materialübersicht LCM-Technologie. Technical report, Vienna, 2021. URL `https://lithoz.com/wp-content/uploads/2022/04/LITHOZ_Materialfolder_DE_web.pdf`. Accessed: May, 2022.

[99] A. Çaglar, B.T. Bal, S. Karakoca, C. Aydın, H. Yılmaz, and S. Sarısoy. Three-Dimensional Finite Element Analysis of Titanium and Yttrium-Stabilized Zirconium Dioxide Abutments and Implants. (26(5):961-9):9, 2011. PMID: 22010077.

[100] S. Liu and Y.C. Shin. Additive manufacturing of Ti6Al4V alloy: A review. *Materials & Design*, 164, February 2019. doi: 10.1016/j.matdes.2018.107552.

[101] T.M.G.J. van Eijden, J.A.M. Korfage, and P. Brugman. Architecture of the human jaw-closing and jaw-opening muscles. *The Anatomical Record*, 248(3):464–474, July 1997. doi: 10.1002/(SICI)1097-0185(199707)248:3<464::AID-AR20>3.0.CO;2-M.

[102] G.J. Pruim, H.J. de Jongh, and J.J. ten Bosch. Forces acting on the mandible during bilateral static bite at different bite force levels. *Journal of Biomechanics*, 13(9):755–763, 1980. doi: 10.1016/0021-9290(80)90237-7.

[103] S. Rues, H.J. Schindler, J. Lenz, and K. Schweizerhof. Calculation of Muscle and Joint Forces in the Masticatory System. In C.A. Motasoares, J.A.C. Martins, H.C. Rodrigues, J.A.C. Ambrósio, C.A.B. Pina, C.M. Motasoares, E.B.R. Pereira, and J. Folgado, editors, *III European Conference on Computational Mechanics*, pages 193–193. Springer Netherlands, Dordrecht, 2006. ISBN 978-1-4020-4994-1. doi: 10.1007/1-4020-5370-3_193.

[104] W.A. Weijs and B. Hillen. Physiological Cross-Section of the Human Jaw Muscles. *Acta anat.*, (121: 31-35):5, 1985. doi: 10.1159/000145938.

[105] A.G. Hannam, I. Stavness, J.E. Lloyd, and S. Fels. A dynamic model of jaw and hyoid biomechanics during chewing. *Journal of Biomechanics*, 41(5):1069–1076, 2008. doi: 10.1016/j.jbiomech.2007.12.001.

[106] H.L. Huang, K.C. Su, L.J. Fuh, M.Y.C. Chen, J. Wu, M.T. Tsai, and J.T. Hsu. Biomechanical analysis of a temporomandibular joint condylar prosthesis during various clenching tasks. *Journal of Cranio-Maxillofacial Surgery*, 43(7):1194–1201, September 2015. doi: 10.1016/j.jcms.2015.04.016.

[107] M.L. Martin, K.J. Travouillon, P.A. Fleming, and N.M. Warburton. Review of the methods used for calculating physiological cross-sectional area (PCSA) for ecological questions. *Journal of Morphology*, 281(7):778–789, July 2020. doi: 10.1002/jmor.21139.

[108] M.S. Commisso, J. Martínez-Reina, J. Ojeda, and J. Mayo. Finite element analysis of the human mastication cycle. *Journal of the Mechanical Behavior of Biomedical Materials*, 41:23–35, January 2015. doi: 10.1016/j.jmbbm.2014.09.022.

[109] T.W.P. Korioth, D.P. Romilly, and A.G. Hannam. Three-dimensional finite element stress analysis of the dentate human mandible. *American Journal of Physical Anthropology*, 88(1):69–96, May 1992. doi: 10.1002/ajpa.1330880107.

[110] G.J. Nelson. Three Dimensional computer modeling of human mandibular biomechanics. Master's thesis, The University of British Columbia, Vancouver, Canada, November 1986.

[111] F. Wieja, G. Jacobs, S. Stein, A. Kopp, K. van Gaalen, N. Kröger, and M. Zinser. Development and validation of a parametric human mandible model to determine internal stresses for the future design optimization of maxillofacial implants. *Journal of the Mechanical Behavior of Biomedical Materials*, 125:104893, January 2022. doi: 10.1016/j.jmbbm.2021.104893.

[112] S. Zhong, Q. Shi, Y. Sun, S. Yang, J. Van Dessel, Y. Gu, X. Chen, H.T. Lübbers, and C. Politis. Biomechanical comparison of locking and non-locking patient-specific mandibular reconstruction plate using finite element analysis. *Journal of the Mechanical Behavior of Biomedical Materials*, 124:104849, December 2021. doi: 10.1016/j.jmbbm.2021.104849.

[113] G.E.J. Langenbach and A.G. Hannam. The role of passive muscle tensions in a three-dimensional dynamic model of the human jaw. *Archives of Oral Biology*, 44(7):557–573, July 1999. doi: 10.1016/S0003-9969(99)00034-5.

[114] D. Bozyel and S. Taşar Faruk. Biomechanical Behavior of All-on-4 and M-4 Configurations in an Atrophic Maxilla: A 3D Finite Element Method. 27, February 2021. doi: 10.12659/MSM.929908.

[115] N. Türker, H.T. Alkiş, S.J. Sadowsky, and U. Şebnem Büyükkaplan. Effects of Occlusal Scheme on All-on-Four Abutments, Screws, and Prostheses: A Three-Dimensional Finite Element Study. 47(1):18–24, 2021. doi: 10.1563/aaid-joi-D-19-00334.

[116] C.H. Gibbs, P.E. Mahan, H.C. Lundeen, K. Brehnan, E.K. Walsh, and W.B. Holbrook. Occlusal forces during chewing and swallowing as measured by sound transmission. *The Journal of Prosthetic Dentistry*, 46(4):443–449, October 1981. doi: 10.1016/0022-3913(81)90455-8.

[117] T.M.G.J. van Eijden. Three-dimensional analyses of human bite-force magnitude and moment. *Archives of Oral Biology*, 36(7):535–539, 1991. doi: 10.1016/0003-9969(91)90148-N.

[118] M. Bakke, B. Holm, B.L. Jensen, L. Michler, and E. Möller. Unilateral, isometric bite force in 8-68-year-old women and men related to occlusal factors. *European Journal of Oral Sciences*, 98(2):149–158, April 1990. doi: 10.1111/j.1600-0722.1990.tb00954.x.

[119] N. Taniguchi, S. Fujibayashi, M. Takemoto, K. Sasaki, B. Otsuki, T. Nakamura, T. Matsushita, T. Kokubo, and S. Matsuda. Effect of pore size on bone ingrowth into porous titanium implants fabricated by additive manufacturing: An in vivo experiment. *Materials Science and Engineering: C*, 59:690–701, 2016. doi: 10.1016/j.msec.2015.10.069.

[120] R.C. Hibbeler. *Technische Mechanik 1*. Pearson Deutschland GmbH, 12. edition, 2012. ISBN 978-3-86894-125-8.

[121] P. Wriggers, U. Nackenhorst, S. Beuermann, H. Spiess, and S. Löhnert. *Technische Mechanik kompakt*. Vieweg + Teubner Verlag, 2006. ISBN 978-3-8351-0087-9. doi: 10.1007/978-3-8351-9066-5.

[122] J. Kováčik. Correlation between Young's modulus and porosity in porous materials. *Journal of Materials Science Letters*, 18:1007–1010, 1999. doi: 10.1023/A:1006669914946.

[123] L.I. Linkow. *Renaissance of the Subperiosteal Implant*, volume 2. XLIBRIS, 2014. ISBN 978-1-499-02851-5.

[124] K.N. Pedersen, H.R. Haanæs, and O. Fæhn. Subperiosteal transmucosal porous ceramic/titanium implants. *International Journal of Oral Surgery*, 8(5):349–355, October 1979. doi: 10.1016/S0300-9785(79)80063-0.

[125] I. Buj-Corral, D. Vidal, A. Tejo-Otero, J.A. Padilla, E. Xuriguera, and F. Fenollosa-Artés. Characterization of 3D Printed Yttria-Stabilized Zirconia Parts for Use in Prostheses. *Nanomaterials*, 11(11):2942, November 2021. doi: 10.3390/nano11112942.

[126] M. Taruna. Prosthodontic Perspective to All-On-4® Concept for Dental Implants. *Journal of Clinical and Diagnostic Research*, 2014. doi: 10.7860/JCDR/2014/9648.5020.

[127] C.H. Turner, J. Rho, Y. Takano, T.Y. Tsui, and G.M. Pharr. The elastic properties of trabecular and cortical bone tissues are similar: results from two microscopic measurement techniques. 32(4):437–441, April 1999. doi: 10.1016/S0021-9290(98)00177-8.

[128] Center for Devices and Radiological Health. Reporting of Computational Modeling Studies in Medical Device Submissions. page 48, September 2016. Docket Number: FDA-2013-D-1530.